Journal of Extracellular Biology

RESEARCH ARTICLE OPEN ACCESS

Stage-Specific Molecular Cargo of Schwann Cell–Derived Extracellular Vesicles is Associated With Peripheral Nerve Repair

Manju Sharma[1] | Supasek Kongsomros[1] | Maulee Sheth[1] | Somchai Chutipongtanate[2] | Leyla Esfandiari[1,3,4,5]

[1]Department of Biomedical Engineering, University of Cincinnati, Cincinnati, Ohio, USA | [2]Division of Epidemiology, Department of Environmental and Public Health Sciences, University of Cincinnati College of Medicine, Cincinnati, Ohio, USA | [3]University of Cincinnati Cancer Center, Cincinnati, Ohio, USA | [4]Department of Environmental and Public Health Sciences, University of Cincinnati, Cincinnati, Ohio, USA | [5]Department of Electrical Engineering and Computer Science, University of Cincinnati, Cincinnati, Ohio, USA

Correspondence: Leyla Esfandiari (esfandla@ucmail.uc.edu)

Received: 10 March 2026 | **Revised:** 21 May 2026 | **Accepted:** 10 June 2026

Keywords: differentiation model | extracellular vesicles | miRNA | peripheral nerve regeneration | repair | Schwann cell

ABSTRACT

Schwann cells (SCs) play a critical role in peripheral nerve regeneration, undergoing dynamic phenotype transitions from myelinating to repair stages following injury. While SC-derived extracellular vesicles (SC-EVs) have emerged as key mediators of intercellular communication during nerve repair, their stage-specific molecular cargo and functional roles remained incompletely understood. Here, we delineate protein, microRNA and long non-coding RNA (lncRNA) landscapes of SC-EVs across distinct differentiation stages, including immature, myelinating, and repair phenotypes, using an in vitro model of primary rat SCs. We show that repair SC-EVs carry distinct microRNAs predicted to modulate genes involved in myelin ensheathment, neuronal differentiation, and neurogenesis. Treatment of immature Schwann cells with repair SC-EVs increased SOX2 expression, suggesting activation of repair-associated Schwann cell responses. Furthermore, modulation of miR-330-5p, miRNA identified in repair SC-EVs, altered SOX2 expression, Schwann cell proliferation, and migration. Repair SC-EVs also contain lncRNAs that may bind and sequester miRNAs, potentially relieving repression of pro-regenerative genes. These findings suggest possible mechanisms by which SC-EVs may regulate Schwann cell repair functions and provide a molecular framework for mechanistic studies.

1 | Introduction

Schwann cells (SCs), the glial cells of the peripheral nervous system (PNS), play a fundamental role in maintaining neuronal structure and function (Bosch-Queralt et al. 2023). These cells form the myelin sheath, which wraps around the axon and enables saltatory conduction of nerve impulses at the nodes of Ranvier, thereby facilitating rapid signal transmission (Rasband and Peles 2021). During development, immature SCs undergo a morphogenetic process called radial sorting, whereby immature SCs segregate large-caliber axons (>1 μm) from mixed bundles in response to signals from both basal lamina and axons (Feltri et al. 2016). This process directs SC differentiation into myelinating SCs, which ensheathe single large-caliber axons in a 1:1 ratio, or non-myelinating SCs, which surround multiple small-caliber axons to form Remak bundles (Feltri et al. 2016).

Manju Sharma and Supasek Kongsomros contributed equally.

This is an open access article under the terms of the Creative Commons Attribution-NonCommercial-NoDerivs License, which permits use and distribution in any medium, provided the original work is properly cited, the use is non-commercial and no modifications or adaptations are made.
© 2026 The Author(s). *Journal of Extracellular Biology* published by Wiley Periodicals LLC on behalf of International Society for Extracellular Vesicles.

Schwann cells also play a critical role in peripheral nerve repair following injury (Oliveira et al. 2023; Rigoni and Negro 2020). Axonal damage triggers the activation of transcription factors such as c-Jun, STAT-3, and Mitf, which reprogram myelinating SCs into a repair phenotype (Benito et al. 2017; Daboussi et al. 2023; Jessen and Mirsky 2021). Elevated c-Jun drives myelin clearance via JNK/c-Jun-dependent myelinophagy (Benito et al. 2017) and concurrently suppresses early growth response protein 2 (EGR2), also known as KROX20, a myelination-promoting transcription factor, to maintain SCs in a repair stage (Parkinson et al. 2004). In parallel, repair SCs facilitate debris clearance by recruiting macrophages through TNF-α and MCP-1 (Martini et al. 2008) and guide the axonal regrowth by aligning into bunger bands, which are regulated by Ephrin-B2/EphB2 signaling and SRY-box transcription factor 2 (Sox2)-mediated N-cadherin redistribution (Parrinello et al. 2010). To promote axon elongation and neuronal survival, repair SCs secrete neurotrophic factors, including glial cell line-derived neurotrophic factor (GDNF), neurotrophin-3 (NT3), brain-derived neurotrophic factor (BDNF), and nerve growth factor (NGF) (Oliveira et al. 2023; Pandey and Mudgal 2022; Parrinello et al. 2010). Upon completion of axonal regrowth, neuregulin-1 type III (Nrg1 III) activates ErbB2/B3 receptors on repair SCs, initiating PI3K/Akt and MAPK/Erk1/2 signaling cascades that restore KROX20 and SRY-box transcription factor 10 (SOX10) expression and enable remyelination (Boerboom et al. 2017).

Most current research on SC-mediated repair has focused on the direct role of cells and cell-cell interactions. However, growing evidence suggests that extracellular vesicles (EVs) also play a critical role in facilitating intercellular communication during peripheral nerve regeneration such as between SCs and neurons (Izhiman and Esfandiari 2024). EVs are nanoscale, lipid bilayer-enclosed particles released by cells that transport bioactive molecules, including proteins, lipids, messenger RNA (mRNA), microRNAs (miRNAs), and long non-coding RNAs (lncRNAs) to mediate intercellular communication over short and long distances (O'Brien et al. 2020; Zhao et al. 2021). EVs also regulate immune responses, promote tissue repair, and modulate disease progression (Chutipongtanate et al. 2022; Kongsomros et al. 2022). In the context of nerve regeneration, EVs from various sources, including mesenchymal stem cells (MSCs), adipose-derived stem cells (ASCs), neurons, olfactory ensheathing cells, and dental pulp stem cells, have been shown to promote axonal growth and myelination (Chen et al. 2023; Luo et al. 2018; Namini et al. 2023; Xia et al. 2019). Schwann cell-derived extracellular vesicles (SC-EVs), in particular, exhibit potent neuroprotective and regenerative properties (Lopez-Leal and Court 2016; López-Leal et al. 2020; Lopez-Verrilli et al. 2013; Wong et al. 2022). SC-EVs enhance retinal ganglion cell survival and axonal growth following optic nerve injury (Zhu et al. 2023) as well as promote motoneuron regeneration (Wu et al. 2020). Mechanistically, SC-EVs deliver regeneration-associated molecules, such as miR-21 (enriched in repair SCs) and miR-23b-3p, both of which promote neurite outgrowth (López-Leal et al. 2020; Xia et al. 2020). Additionally, SC-EVs carry TNFR1, which binds and sequesters excess TNFα, thereby limiting inflammation and promoting macrophage polarization toward a pro-repair phenotype, ultimately supporting tissue regeneration (Gonias and Campana 2023). These findings emphasize the regenerative potential of SC-EVs.

Despite promising evidence, the functional role of SC-EVs in nerve repair remains incompletely understood, particularly regarding their contributions at distinct stages of SC differentiation. Transcriptomics analyses can identify potential regulatory candidates. Here, we aim to characterize the molecular landscape of SC-EV cargo across Schwann cell differentiation stages to guide future mechanistic investigations. We hypothesize that SC-EVs, whether released from repair SCs at injury sites or from adjacent uninjured myelinating SCs, act as mediators of nerve regeneration by delivering stage-specific molecular cargo to neurons and SCs, thereby coordinating the repair process. In this study, we investigated the roles of SC-EVs across three differentiation stages: immature, myelinating, and repair SCs. By isolating and characterizing EVs from each phenotype, we performed western blotting and comparative transcriptomic profiling to identify regeneration-associated proteins and RNAs, and conducted functional assays demonstrating that repair SC-EVs induce regenerative transcriptional responses in recipient immature SCs. Our findings reveal how SC-EVs orchestrate regeneration through stage-specific molecular cargo and provide mechanistic insights into SC-EV-mediated intercellular signaling in peripheral nerve repair.

2 | Results

2.1 | Validation and Characterization of an in Vitro Schwann Cell Differentiation Model

Schwann cells (SCs) are essential for peripheral nerve repair, undergoing reprogramming from a myelinating to a repair phenotype in response to injury. To investigate the molecular mechanisms underlying this transition and EV-mediated communication, we utilized a previously established in vitro differentiation model (Figure 1A) that recapitulates key stages of SC maturation and reversion (Zou 2023). Primary rat SCs were treated with dbcAMP to simulate axonal contact and activate signaling cascades that induce differentiation into the myelinating phenotype (Leitman et al. 2011). Subsequent dbcAMP withdrawal prompted reversion to the repair phenotype (Monje 2018; Zou et al. 2023).

Distinct morphological changes of SC differentiation were observed under phase-contrast and actin-stained imaging (Figure 1B,C). Immature SCs exhibited an undifferentiated, spindle-shaped, elongated morphology, while myelinating SCs were bigger, rounded, and flattened appearance with reduced cytoskeletal organization, consistent with the previous report (Leitman et al. 2011), indicating activation of the myelination process. Upon dbcAMP withdrawal, repair SCs reverted to an elongated morphology and re-established organized actin filaments, resembling the immature SC phenotype.

To further evaluate stage-specific characteristics, we assessed the expression of key markers by immunofluorescence (Figure 1D) and western blot analysis (Figure 1E). Immature SCs expressed transcription factors c-Jun and SOX2 and the neurotrophin receptor $p75^{NTR}$, indicative of a proliferative, undifferentiated stage. Myelinating SCs showed upregulation of KROX20 and myelin basic protein (MBP), hallmarks of myelin sheath for-

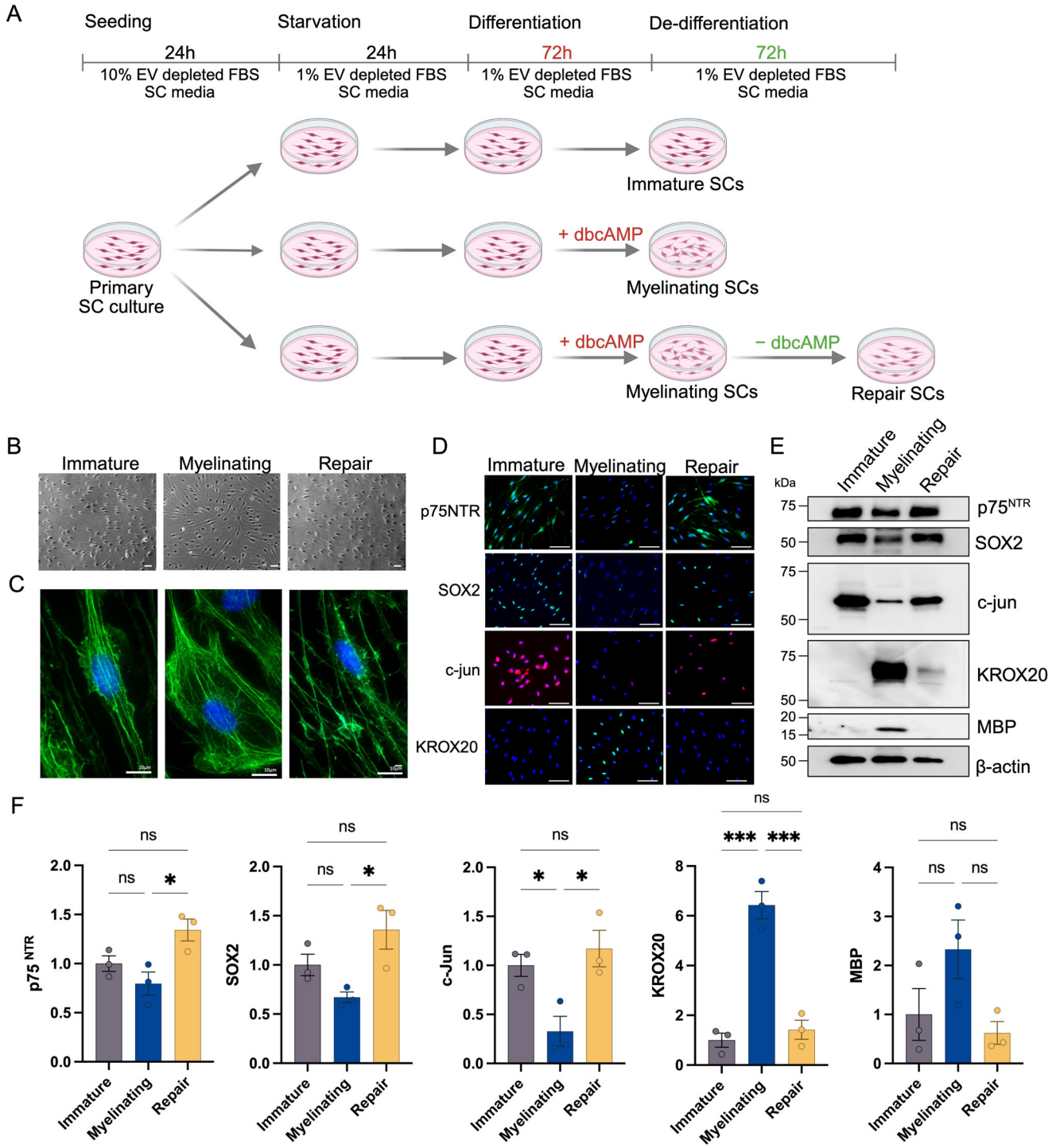

FIGURE 1 | Schwann cell differentiation and molecular marker validation. (A) Schematic of the in vitro differentiation model used to induce Schwann cells (SCs) myelination, followed by reversion to a repair phenotype. Rat primary SCs were treated with 1 mM dbcAMP in rat SC basal media for 72 h to induce differentiation into myelinating SCs, followed by dbcAMP withdrawal to reprogram into repair SCs. (B) Phase contrast and (C) phalloidin-stained super-resolution fluorescence imaging illustrates morphological differences and cytoskeletal organization in immature, myelinating, and repair SCs. Scale bars: 20 μm and 10 μm, respectively. (D) Immunofluorescence staining for SC-specific markers $p75^{NTR}$, SOX2, c-Jun, and KROX20 shows distinct molecular profiles for differentiation stages. Immature SCs express high $p75^{NTR}$, c-Jun, and Sox2; myelinating SCs express KROX20; repair SCs re-express immature proliferative markers. Scale bars: 100 μm. Immunofluorescence quantification of KROX20-positive cells is shown in Figure S1 (E) Western blot analysis confirms different expression patterns of SC markers across distinct differentiation stages (the full-length blot images were available in Figure S2). (F) Western blot quantification shows downregulation of $p75^{NTR}$, c-Jun, and Sox2 as normalized to actin in myelinating SCs, with significant upregulation in repair SCs. KROX20 and MBP were elevated in myelinating SCs. The data are presented as the mean ± SEM of three biological replicates. Statistical analysis was performed by using one-way ANOVA with Tukey's multiple comparisons test: * $p < 0.05$, ** $p < 0.005$, and *** $p < 0.001$, ns, not significant.

mation. In contrast, repair SCs upregulated c-Jun, SOX2, and $p75^{NTR}$, and concurrently repressed KROX20, consistent with a regenerative, dedifferentiation stage. Quantification of protein expression confirmed significant upregulation of $P75^{NTR}$, SOX2, and c-Jun expressions in repair SCs, and increased expression of KROX20 and MBP in myelinating SCs (Figure 1F). Immunofluorescence analysis confirmed efficient myelination induction, with ~75% of cells expressing KROX20 after dbcAMP treatment; this percentage subsequently declined to ~5% during the repair stage (Figure S1). Together, these findings validate the in vitro SC differentiation model as a robust platform for dissecting molecular transitions and SC-EV-mediated communication during nerve injury and regeneration.

2.2 | Transcriptomic Profiling Reveals Molecular Pathways Driving Schwann Cell Myelination and Repair

To elucidate molecular mechanisms governing SC differentiation, we performed poly(A) RNA sequencing on SCs at distinct differentiation stages; immature, myelinating, and repair phenotypes, with RNA integrity confirmed in Figure S3. The heatmap with hierarchical clustering showed discrete gene expression profiles among these states (Figure 2A). Principal component analysis (PCA) revealed clear transcriptional segregation between immature and myelinating SCs (Figure 2B), as well as between myelinating and repair SCs (Figure 2C). Notably, immature and repair SCs exhibited overlapping transcriptional signatures (Figure 2D), consistent with a partial reversion to an immature-like stage during nerve repair (Bosch-Queralt et al. 2023; Quintes and Brinkmann 2017).

During differentiation into myelinating SCs, differential expression analysis identified 726 upregulated and 947 downregulated genes compared to immature SCs (Figure 2E, full data in Table S1). Myelinating SCs exhibited significant upregulation of KROX20/Egr2 and MBP genes, both essential for myelin formation. Gene ontology (GO) enrichment analysis identified the top 10 biological pathways enriched in myelinating SCs, including Eph/ephrin signaling, myelination, receptor tyrosine kinase signaling, neuron projection development, and sodium/potassium ion transmembrane transport (Figure 2H, full data in Table S2). Gene set enrichment analysis (GSEA) corroborated enrichment in pathways associated with myelination, myelin maintenance, and membrane potential regulation, indicating the specialized role of myelinating SCs in axon wrapping, myelin sheath formation, and signal propagation (Figure S4A).

Conversely, reprogramming to repair SCs was characterized by 430 upregulated and 380 downregulated genes compared to the myelinating stage (Figure 2F, full data in Table S3). This transition was marked by downregulation of myelin-related genes, including MBP and KROX20/Egr2, and upregulation of transcription factors c-Jun, SOX2, and neurotrophin receptor $p75^{NTR}$/Ngfr, indicating activation of a proliferative state (Figure 2F). GO analysis identified the enriched pathways involved in axon guidance, which facilitates axon regrowth and SC migration, as well as PI3K/Akt signaling, ERK1/2 cascade, and MAPK activation, which promote cell survival and regeneration. Additional enriched pathways included negative regulation of apoptosis, essential for preventing neuronal death, and positive regulation of cell migration, which directs SCs to injury sites (Figure 2I, full data in Table S4). GSEA identified gene sets associated with neurogenesis, neuroinflammatory responses, growth activity, and apoptosis regulation, indicating their roles in nerve repair, inflammation response, and neuroprotection (Figure S4B). Collectively, these transcriptomic data delineate stage-specific regulatory mechanisms that direct the functional specialization of SCs in myelinating and repair stages.

2.3 | Isolation and Characterization of Extracellular Vesicles From Schwann Cells Across Distinct Differentiation Stages

To elucidate the role of SC-EVs in nerve repair, EVs were isolated from the conditioned media of immature, myelinating, and repair-stage SCs using an indirect dielectrophoresis-based microfluidic device (iDEP) (Figure 3A), which we have previously established (Sharma et al. 2023; Shi and Esfandiari 2022; Shi et al. 2019; Shi et al. 2018). The presence of EVs was validated according to the Minimum Information for Studies of Extracellular Vesicles (MISEV2023) guidelines (Welsh et al. 2024). TEM with negative staining of EVs purified from all three SC stages showed cup-shaped vesicle morphology (Figure 3B). Nanoparticle tracking analysis (NTA) revealed a consistent mean diameter less than 200 nm of SC-EVs from all differentiation stages, characteristic of small EVs (Figure 3C) (Welsh et al. 2024). Western blotting confirmed the presence of common EV markers including CD63, HSP70, and TSG101, and the absence of negative marker Calnexin (Figure 3D, the full-length western blot images are available in Figure S5. In addition, to reduce potential carryover of EVs generated during earlier differentiation stages, cells were extensively washed during stage transitions prior to EV collection, and differentiation efficiency was confirmed prior to EV isolation (Figure S1). These characterization data support the integrity and specificity of EV preparations for further analyses.

2.4 | Myelinating Schwann Cell-Derived Extracellular Vesicles Carry Regeneration-Associated Proteins

To confirm the SC origin of EVs at different differentiation stages, super-resolution microscopy was employed to identify $CD63^{+}$ vesicles co-expressing the SC marker $p75^{NTR}$ (Figure 4A). Next, we utilized western blotting to further characterize their protein cargo. As expected, MBP was highly enriched in myelinating SC-EVs, reflecting the identity of their parental cells (Figure 4B,C). Interestingly, SOX2 and $p75^{NTR}$, markers of proliferation and repair, were enriched in myelinating SC-EVs despite relatively low expression in myelinating SCs, while their levels were reduced in SC-EVs from immature and repair stages compared to their cellular sources (as shown in Figure 1E). These findings suggest that myelinating SC-EVs selectively package proteins associated with repair-related signaling pathways. However, the functional contribution of these EV-associated proteins to peripheral nerve repair requires further investigation.

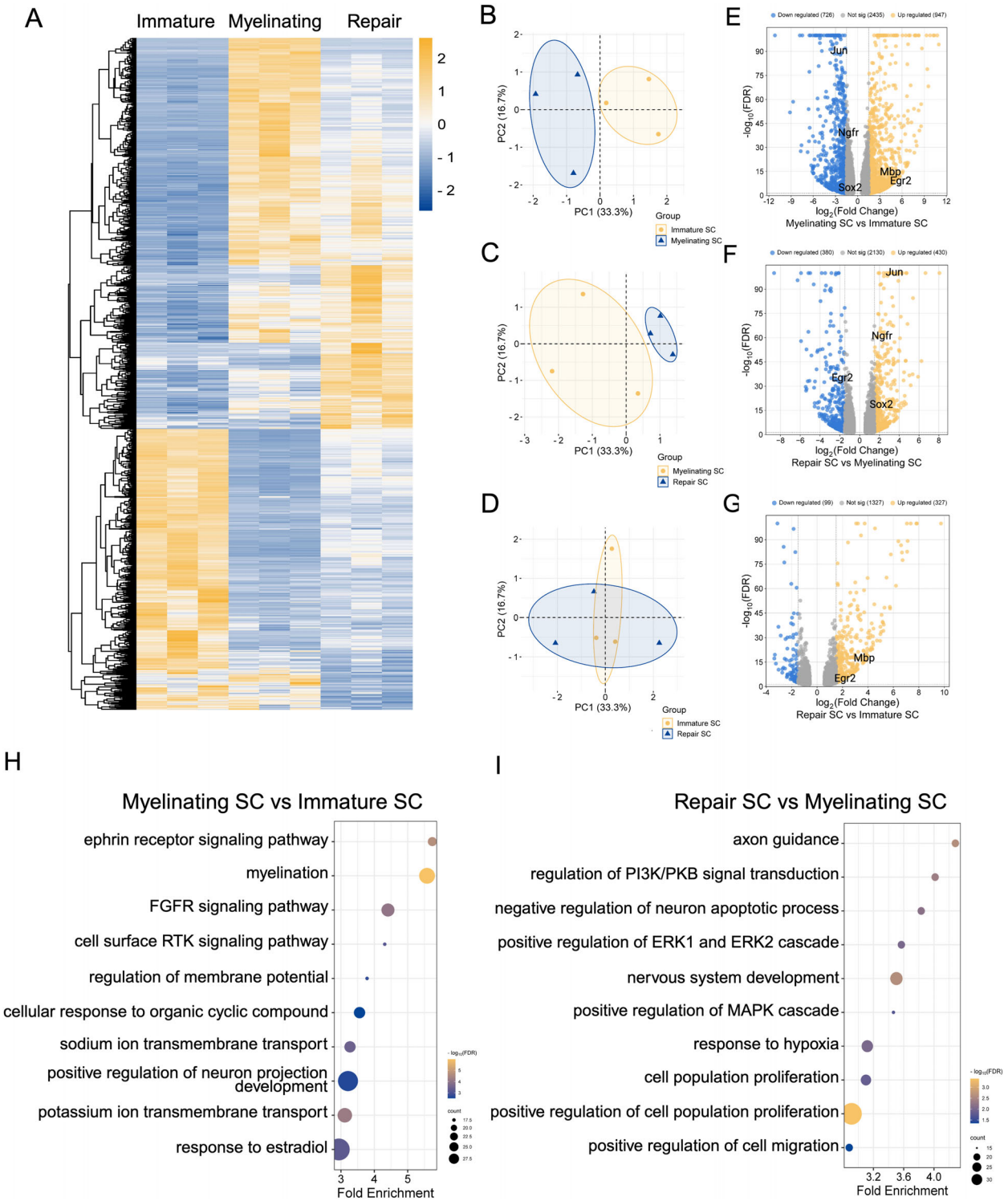

FIGURE 2 | Transcriptomic analysis of Schwann cell differentiation. (A) Heatmap with hierarchical clustering shows significant differential gene expression profiles across immature, myelinating, and repair SCs. Each row represents an individual mRNA, with color intensity indicating expression levels (blue: downregulated; yellow: upregulated). Principal component analysis (PCA) reveals distinct clustering of transcriptomic profiles between myelinating and immature SCs (B), repair and myelinating SCs (C), and overlapping profiles between repair and immature SCs (D). Volcano plots demonstrate differentially expressed genes between SC stages, with upregulated (yellow) and downregulated (blue) genes. (E) Myelinating SCs vs. immature SCs (baseline = immature SCs). (F) Repair SCs vs. myelinating SCs (baseline = myelinating SCs). (G) Repair SCs vs. immature SCs (baseline = immature SCs). Genes with $\log_2$ fold change ≥ 1.5 or ≤ -1.5 and q-value ≤ 0.05 are considered significantly differentially expressed. (H) Top 10 gene ontology (GO) enrichment analysis of upregulated genes identifying biological processes associated with myelinating SCs compared to immature and repair SCs. (I) Top 10 GO enrichment analysis of upregulated genes identifying biological processes associated with repair SCs compared to myelinating SCs.

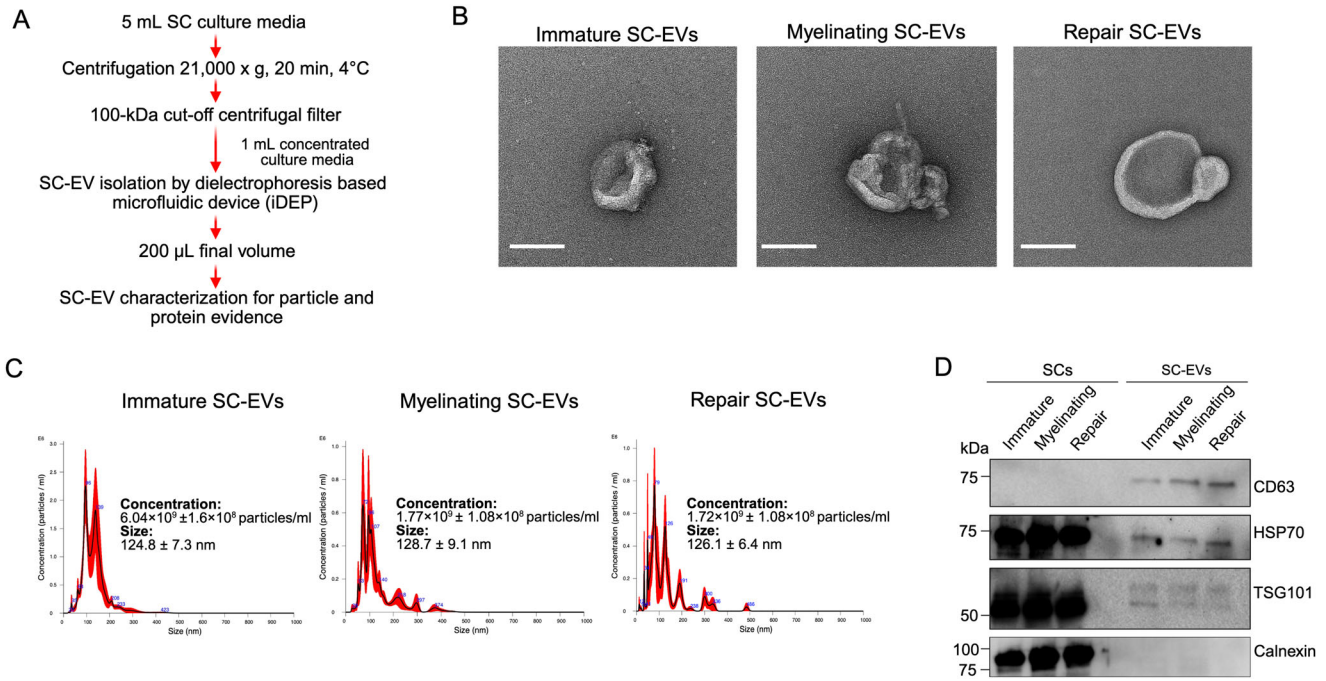

FIGURE 3 | SC-EV isolation and characterization. (A) A schematic diagram represents SC-EV isolation process. (B) Transmission electron microscopy shows a cup-shape morphology of EVs isolated from immature, myelinating, and repair SCs. Scale bar, 100 nm. (C) Nanoparticle tracking analysis (NTA) showing EV size distributions and concentrations, with average diameters of 124.8 ± 7.3 nm, 128.7 ± 9.1 nm, and 126.1 ± 6.4 nm, and concentrations of 6.04×10^9, 1.77×10^9, and 1.72×10^9 particles/ml for immature, myelinating, and repair SCs, respectively. (D) Western blot analysis confirming the presence of EV-specific markers CD63, TSG101, HSP70, and calnexin across all stages.

2.5 | Stage-Specific SC-EV miRNAs Regulate Pathways Associated With Nerve Regeneration

To determine whether SC-EVs carry stage-specific miRNAs associated with nerve regeneration, we performed small RNA sequencing on EVs isolated from SC at three differentiation stages. RNA quality, assessed by Bioanalyzer, is shown in Figure S7. RNA quality assessment confirmed good integrity, and three biological replicates per group, consistent with standard RNA-seq practice (Conesa et al. 2016), support the reliability of the dataset. Heatmap with hierarchical clustering of significantly expressed miRNAs revealed stage-specific expression profiles (Figure 5A), indicating selective miRNA cargo associated with each SC stage. We selected differentially expressed miRNAs from this heatmap, focusing on those upregulated or downregulated in repair SC-EVs compared to myelinating SC-EVs, as this transition represents a shift from axonal maintenance to regenerative function. In total, 52 downregulated and 67 upregulated mature miRNAs were identified in repair SC-EVs (Table S5). Target prediction using the intersection between miRWalk and miRDB revealed 2,541 shared target genes of downregulated miRNAs and 2,325 targets of upregulated miRNAs (Figures 5B,F).

To validate the sequencing-based miRNA findings, we selected the top two downregulated miRNAs (miR-503-3p and miR-330-5p) and the top upregulated miRNA (miR-223-3p) identified in repair versus myelinating SC-EVs (Table S6) and performed quantitative Reverse Transcription Polymerase Chain Reaction (qRT-PCR) analysis. Consistent with the sequencing results, miR-503-3p and miR-330-5p were significantly reduced in repair SC-EVs compared with myelinating SC-EVs, whereas miR-223-3p was significantly elevated (Figure S8). These data support the reliability of the differential miRNA signatures identified in the sequencing dataset.

To assess the functional relevance of these miRNAs, we performed pathway enrichment analysis using DAVID. Gene ontology (GO) analysis of target genes of downregulated miRNAs in repair SC-EVs revealed significant enrichments in neuronal structures including dendrites, axons, neuronal cell bodies, and synapses (Figure 5C, full data in Table S7) as well as biological processes involved in regulation of signaling (GO: BP cluster 1), neurogenesis (GO: BP cluster 2), neuron morphogenesis (GO: BP cluster 3) and protein localization (GO: BP cluster 4) (Figure 5D, full data in Table S8). Reactome pathway enrichment showed involvement in signal transduction, MAPK signaling (including ERK/MAPK targets and MAP kinase activation), receptor tyrosine kinase signaling, and transmembrane transport (Figure 5E, full data in Table S9).

Upregulated miRNAs in repair SC-EVs were also linked to target genes; presumably suppressed in recipient cells, involved in neuronal cell bodies, synapses, and dendritic structures (Figure 5G, full data in Table S7). Gene ontology analysis further identified enrichment of biological processes related to neuron projection morphogenesis (GO: BP cluster 1), transcriptional activation (GO: BP cluster 2), glycosylation (GO: BP cluster 3), and myelination (GO: BP cluster 4). (Figure 5H, full data in Table S8). Reactome pathway analysis revealed significant enrichment in signaling pathways related to PI3K/AKT signaling, RHO GTPase pathways, TGFB and WNT signaling, transcription factor activation (including AP-1), ion homeostasis, and

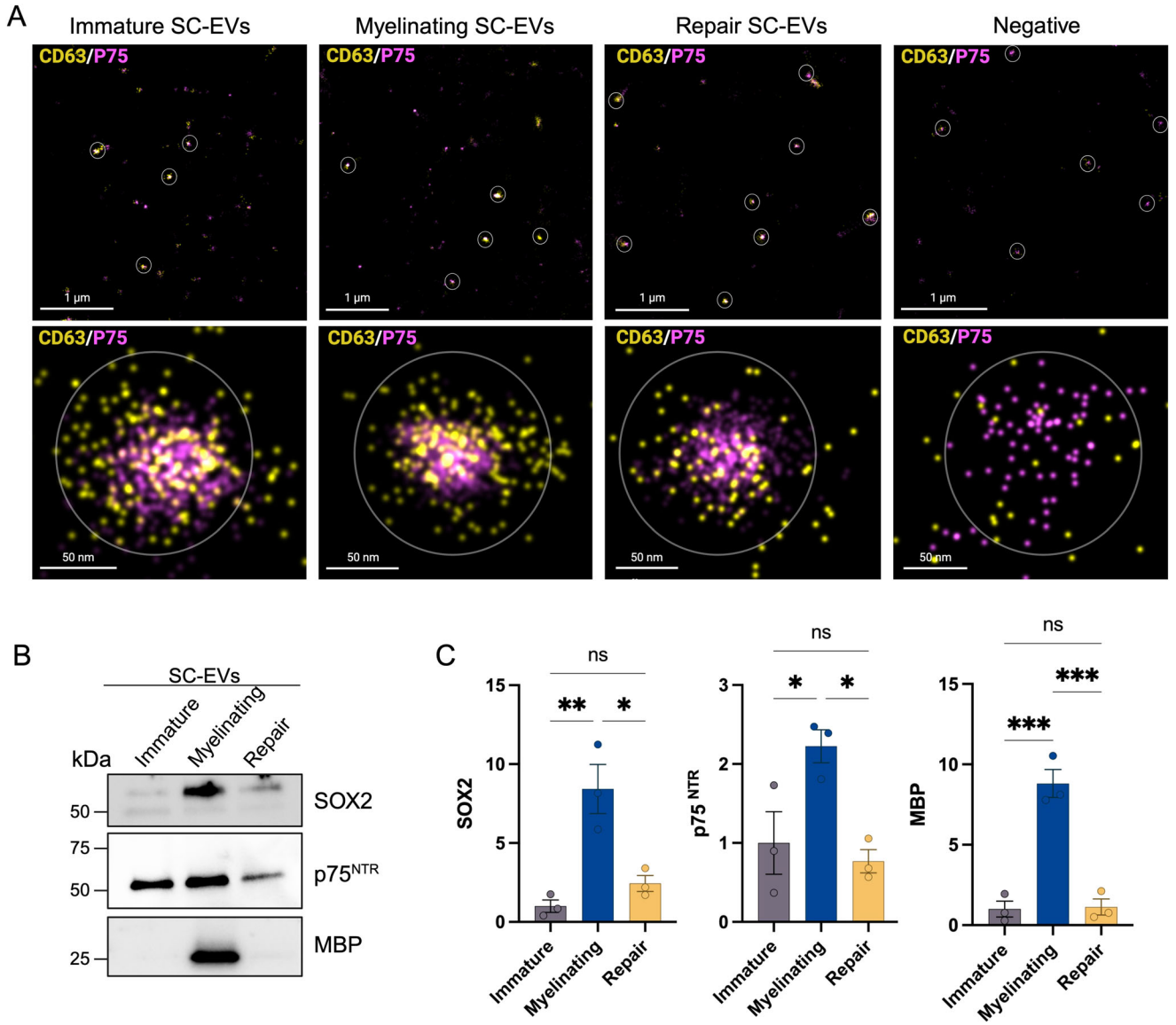

FIGURE 4 | Stage-specific protein cargo in Schwann cell-derived extracellular vesicles (SC-EVs). (A) Representative direct stochastic optical reconstruction microscopy (dSTORM) showing positive CD63 signals co-expression with SC marker $p75^{NTR}$ on a single particle SC-EV. Upper panels show lower magnification views (scale bar, 1 μm) with circled regions indicating single EVs positive for both markers. Lower panels present high-magnification views of representative EVs (scale bar, 50 nm). (B) Western blot analysis of stage-specific EV marker SOX2, $p75^{NTR}$, and MBP in EVs derived from immature, myelinating, and repair SCs (the full-length blot images are available in Figure S6). (C) Quantification of EV-associated protein expression demonstrating significant enrichment of SOX2, $p75^{NTR}$, and MBP markers in EVs derived from myelinating SCs. Data presented as mean ± SEM ($n = 3$ biological replicates per group). Statistical analysis was performed by using one-way ANOVA with Tukey's multiple comparisons test: * $p < 0.05$, ** $p < 0.005$, and *** $p < 0.001$, ns, not significant.

cell death signaling (Figure 5I, full data in Table S9). Overall, our data demonstrate that SC-EVs exhibit stage-specific miRNA cargo capable of modulating gene expression in recipient cells, thereby contributing to distinct roles in peripheral nerve regeneration.

2.6 | Repair SC-EVs Contain lncRNAs That May Modulate miRNA Activity

Long non-coding RNAs (lncRNAs) regulate gene expression through diverse mechanisms, including by acting as competitive endogenous RNAs or sponges that sequester miRNAs and modulate downstream targets (Chen and Kim 2024; Chuang et al. 2023). To explore the presence of regulatory lncRNAs in SC-EVs, we performed expression profiling across immature, myelinating, and repair SC-EVs. RNA quality was verified in Figure S7. A heatmap of the most abundantly expressed lncRNAs in repair SC-EVs is shown in Figure 6A (expression data in Table S10); although these lncRNAs were not statistically differentially expressed, they were selected based on relative abundance and remain uncharacterized in current databases. To assess their potential function as miRNA sponges, we selected upregulated clusters from the heatmap and performed miRNA-lncRNA interaction analysis using miRanda, focusing on high-affinity binding pairs (total score >140; minimum energy < –20 kcal/mol) (Marín

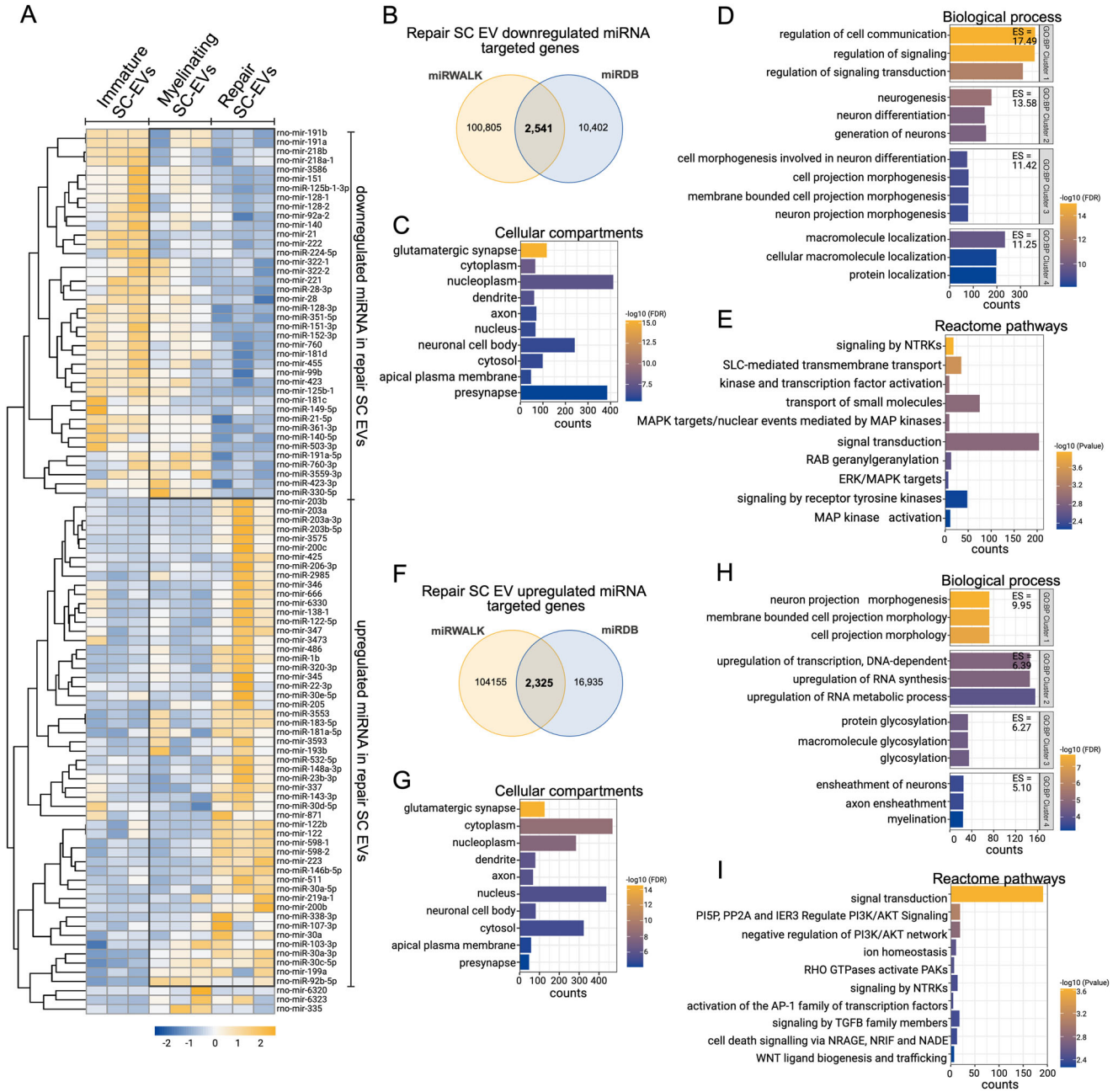

FIGURE 5 | miRNA profiling of Schwann cell-derived extracellular vesicles (SC-EVs). (A) Heatmap showing hierarchical clustering shows differentially expressed miRNAs in SC-EVs from immature, myelinating, and repair SCs. Each row represents an individual miRNA, with color intensity indicating relative expression levels (blue: downregulated; yellow: upregulated). (B, F) Venn diagrams illustrating overlap between predicted target genes identified by miRWalk and miRDB databases for downregulated (B) and upregulated (F) miRNAs in repair SC-EVs. The intersection region indicates commonly predicted targets. (C, G) Gene Ontology (GO) Cellular component analysis of predicted target genes associated with downregulated (C) and upregulated (G) miRNAs in repair SC-EVs. (D, H) GO Biological process enrichment analysis of target genes corresponding to downregulated (D) and upregulated (H) miRNA in repair SC-EVs. (E, I) Reactome functional pathway enrichment analysis of predicted target genes associated with downregulated (E) and upregulated (I) miRNAs in repair SC-EVs.

and Vanícek 2011). This analysis focused on miRNAs associated with neurogenesis that were downregulated in repair SC-EVs. Upregulated lncRNAs were then predicted to bind these miRNAs. (Figure 6B, full data in Table S11). These results support the possibility that repair SC-EVs may deliver lncRNAs which could bind and sequester miRNAs, lifting their repression of genes associated with regenerative pathways.

2.7 | Repair SC-EV Treatment Increases SOX2 Expression in Recipient Schwann Cells

To determine whether the stage-specific molecular signatures of repair SC-EVs translate into functional effects, we assessed their ability to induce repair-associated responses in immature Schwann cells. Since SOX2 is transiently upregulated after nerve

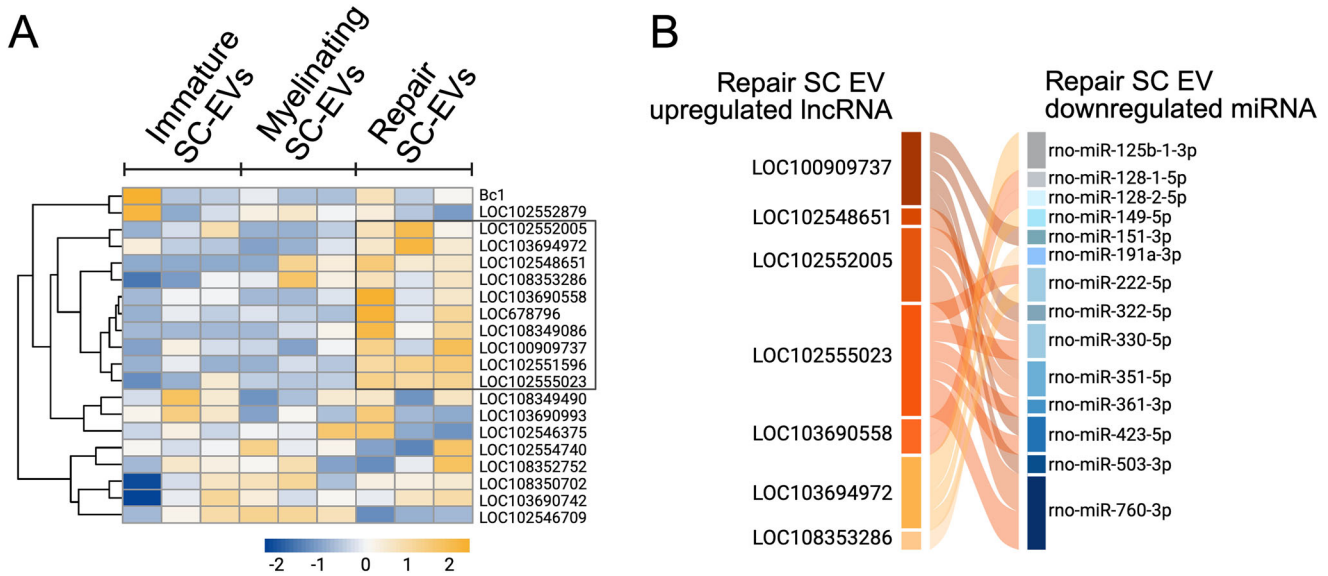

FIGURE 6 | lncRNA expression and predicted miRNA interactions in repair SC-EVs. (A) Heatmap with hierarchical clustering of the most abundant lncRNAs in repair SC-EVs. Each row represents an individual lncRNA, with color intensity indicating relative expression (blue: low; yellow: high). (B) Sankey diagram showing predicted interactions between upregulated lncRNAs in repair SC-EVs and downregulated miRNAs, based on miRanda binding predictions.

injury and a key driver of the repair phenotype (Li et al. 2021), we used SOX2 as a marker of repair-associated transcriptional activation. Primary immature Schwann cells were treated with EVs derived from all three stages (immature, myelinating, and repair SCs), as well as with media alone as a control for 72 h (Figure 7A). Western blot analysis showed that only repair SC-EVs significantly increased SOX2 protein levels compared with the control or EVs from other stages (Figure 7B,C). This functional effect suggests that repair SC-EVs may influence repair-associated transcriptional responses in immature recipient Schwann cells.

2.8 | MiR-330-5p Regulates SOX2 Expression, Schwann Cell Proliferation, and Migration

To further investigate the mechanisms associated with repair SC-EV-mediated SOX2 induction, we examined candidate miRNAs identified in repair SC-EVs. Among the differentially expressed miRNAs, miR-330-5p and miR-503-3p were enriched in myelinating SC-EVs but reduced in repair SC-EVs (Figure S8). To evaluate their functional roles, RT4-D6P2T Schwann cells were transfected with miR-330-5p or miR-503-3p mimics and inhibitors. Western blot analysis demonstrated that miR-330-5p overexpression reduced SOX2 expression, whereas inhibition of miR-330-5p restored the expression of SOX2 (Figure 8A). In contrast, transfection with -503-3p mimics or inhibitors did not significantly alter SOX2 expression (Figure 8A). Since SOX2 is associated with cell proliferation and repair responses (Li et al. 2021; Zhang et al. 2020), we examined the functional effects of miRNA modulation. Consistent with the observed changes in SOX2 expression, miR-330-5p mimic significantly decreased Schwann cell proliferation, whereas miR-330-5p inhibition restored proliferation to control levels (Figure 8B). In contrast, miR-503-3p mimic showed only a slight increase on proliferation while miR-503-3p inhibitor restored proliferation toward control levels (Figure 8B). Wound healing assays further demonstrated that miR-330-5p overexpression delayed wound closure at 12 h and 24 h, whereas miR-330-5p inhibition promoted wound closure (Figure 8C–D). In comparison, miR-503-3p mimic and inhibitor had minimal effects on wound closure (Figure 8C–D). Collectively, the results indicate that miR-330-5p contributes to repair-associated Schwann cell functions by regulating SOX2 expression, proliferation, and migration.

3 | Discussion

Following nerve injury, SCs undergo a dynamic phenotypic reprogramming, transitioning from a myelinating to a repair stage to support nerve regeneration. Emerging evidence suggests that SC-EVs are crucial mediators of SC-neuron communication (Izhiman and Esfandiari 2024; Lopez-Leal and Court 2016; Lopez-Verrilli et al. 2013; Wong et al. 2022). However, the molecular cargo and functional divergence of SC-EVs at distinct differentiation stages remain incompletely understood. Here, we comprehensively profiled proteins, miRNAs, and lncRNAs in SC-EVs derived from immature, myelinating, and repair phenotypes, revealing stage-specific regulatory signatures associated with peripheral nerve regeneration.

We first validated the differentiation stages of immature, myelinating, and repair SCs (Zou 2023) by confirming characteristic morphology and molecular markers (Figure 1). Immature SCs showed high expression of c-Jun, SOX2, and $p75^{NTR}$; markers associated with proliferation, developmental plasticity, and regenerative potential (Balakrishnan et al. 2016; Leitman et al. 2011; Liu et al. 2015; Zou 2023). Myelinating SCs showed increased KROX20 and MBP expression together with morphological maturation (Balakrishnan et al. 2016; Leitman et al. 2011; Liu et al. 2015). Upon dedifferentiation, repair SCs re-acquired immature-like morphology and re-expressed regenerative markers, high-

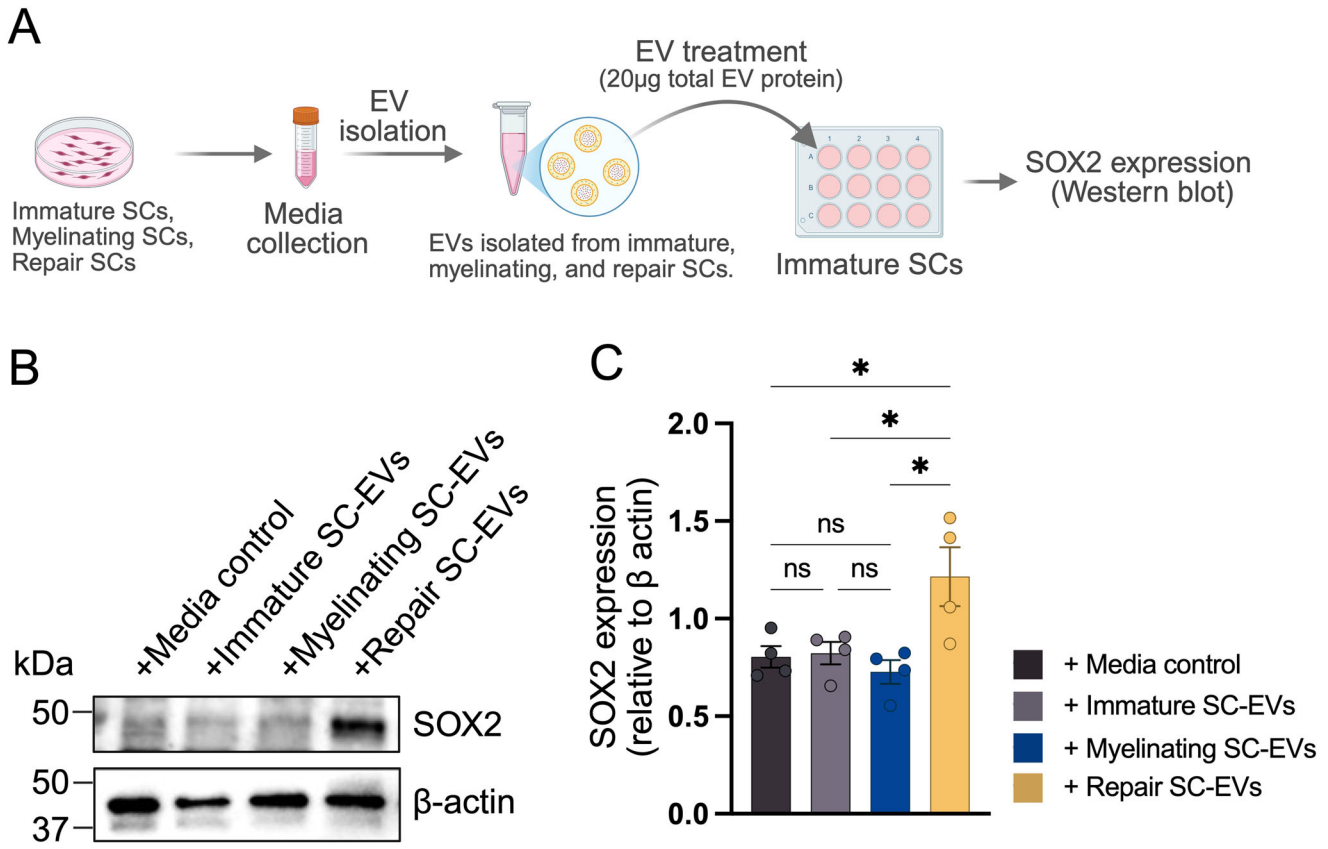

FIGURE 7 | Repair SC-EVs induce SOX2 expression in recipient Schwann cells. (A) Schematic of the experimental workflow. Primary immature Schwann cells were seeded in 12-well plates and cultured in growth medium containing EV-depleted FBS for 24 h prior to treatment. EVs were isolated from media collected from immature, myelinating, and repair Schwann cells and applied to recipient cells at 20 µg EV protein (~5×10^3 EVs per cell). SOX2 expression was assessed 72 h after treatment by western blot. (B) Representative western blot analysis showing SOX2 protein expression in Schwann cells treated with EVs from each differentiation stage or media alone (control). β-actin served as the loading control. (C) Quantification of SOX2 protein levels relative to β-actin. Repair SC-EV treatment significantly increased SOX2 expression compared with the control group or EVs from other stages. Data presented as mean ± SEM ($n = 3$ biological replicates per group). Statistical analysis was performed by using one-way ANOVA with Tukey's multiple comparisons test: * $p < 0.05$, ** $p < 0.005$, and *** $p < 0.001$, ns, not significant.

lighting SC plasticity in response to injury-associated signals (Boerboom et al. 2017; Nocera and Jacob 2020; Quintes and Brinkmann 2017; Yao and Wang 2020; Zou 2023). Transcriptomic analyses further supported these phenotypic transitions. Myelinating SCs displayed enrichment of myelin-related genes, including KROX20/Egr2 and MBP, and signaling pathways linked to myelination, such as receptor tyrosine kinase and Eph/ephrin signaling. Upregulation of ion channel-related genes further reflected the functional maturation of myelinating SCs. (Figure 2H) (Boerboom et al. 2017; Bosch-Queralt et al. 2023; Muppirala et al. 2021). In contrast, repair SCs showed enriched signaling pathways linked to proliferation, axon guidance, anti-apoptosis, and immunomodulation (Figure 2I), consistent with their role in supporting regeneration (Jessen and Mirsky 2021, 2022). This was accompanied by reactivation of c-Jun, SOX2, and $p75^{NTR}$, and downregulation of myelin-specific genes; the hallmarks of the repair phenotype.

SC-EVs carry stage-specific molecular cargo that mirrors the phenotype of their cells of origin. Notably, EVs released by myelinating SCs were enriched in regenerative proteins, including SOX2 and $p75^{NTR}$, despite relatively low intracellular expression at this stage (Figures 1E and 4B). This discrepancy points to selective cargo-sorting mechanisms, whereby EV content does not directly reflect cellular protein abundance (Chen et al. 2022; Dixson et al. 2023). One possibility is that SCs utilize EVs to expel proteins no longer required intracellularly, consistent with the dual roles of EVs in both intercellular communication and cellular waste management (M et al. 2017; Zou et al. 2023). The enrichment of SOX2 and $p75^{NTR}$ within myelinating SC-EVs suggests their potential involvement in nerve repair. Since myelinating SCs mostly present near injury sites, their EVs may serve as readily accessible sources of regenerative signals during the early phases of nerve regeneration. This mechanism is supported by previous studies demonstrating that SOX2-contained EVs promote neurite extension and axonal regeneration (Chen, Chang, et al. 2022; López-Leal et al. 2020), and $p75^{NTR}$ enhances neuronal survival (Follis et al. 2021). Nevertheless, functional validation is required to confirm whether EV-contained SOX2 and $p75^{NTR}$ proteins actively contribute to nerve regeneration in this context. Furthermore, studies investigating selective cargo loading and sorting mechanisms in Schwann cells will be important for advancing our understanding of SC-EV biology.

A particular novel aspect of our study is the identification of stage-specific miRNA cargo within repair SC-EVs. Small

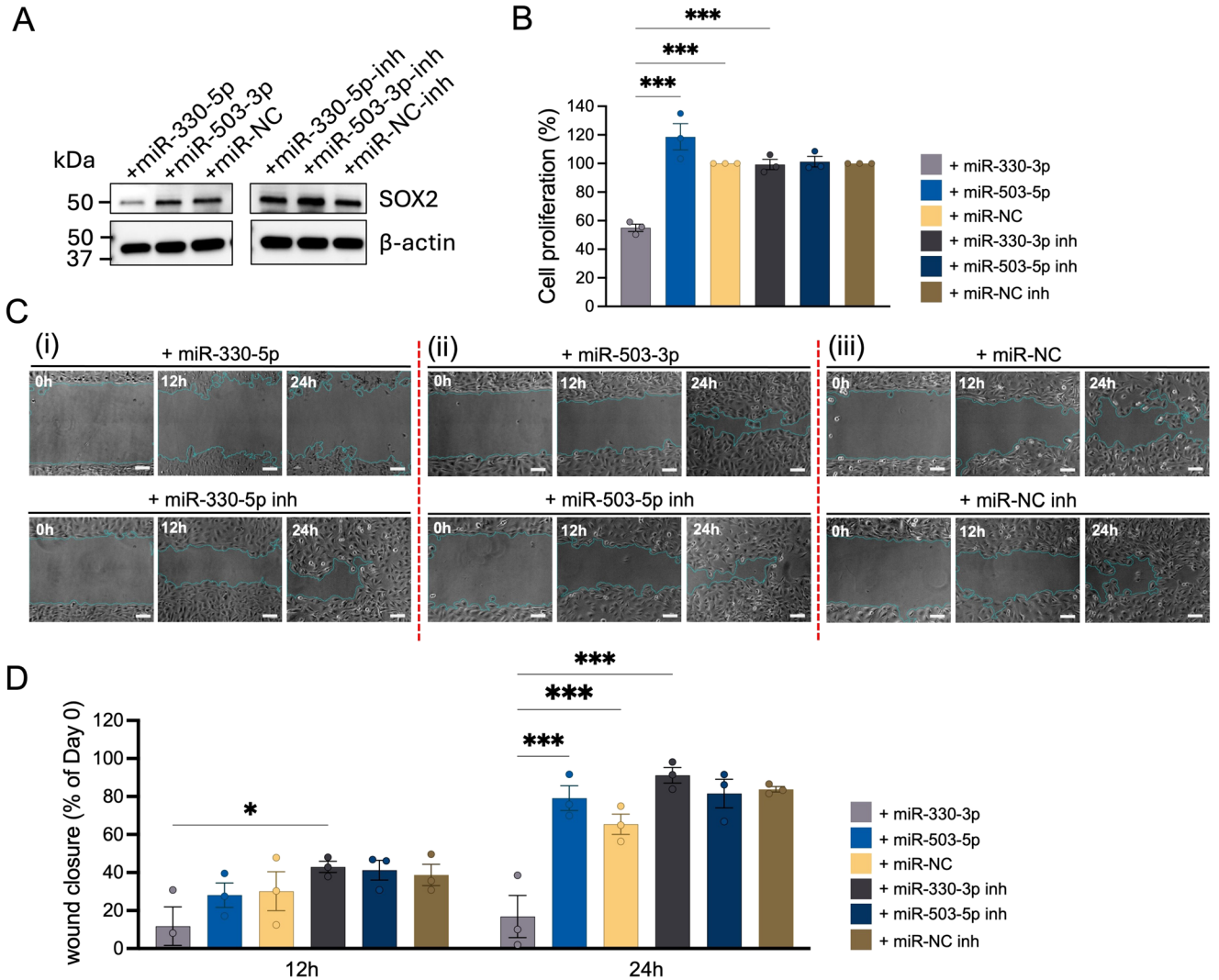

FIGURE 8 | Functional analysis of miR-330-5p and miR-503-3p in SOX2 expression, Schwann cell proliferation, and migration. (A) Representative Western blot analysis of SOX2 expression in RT4-D6P2T Schwann cells transfected with miR-330-5p or miR-503-3p mimics, inhibitors, and corresponding non-targeting negative control mimics (miR-NC) or negative control inhibitors (miR-NC inh) lacking homology to known miRNA sequences. β-actin was used as the loading control. (B) Quantification of Schwann cell proliferation using MTT assay following transfection with miR-330-5p or miR-503-3p mimics and inhibitors. (C) Representative images from wound healing assays at 0 h, 12 h, and 24 h following transfection with (i) miR-330-5p mimic/inhibitor, (ii) miR-503-3p mimic/inhibitor, and (iii) negative controls. Cyan outlines indicate wound boundaries. Scale bars: 100 μm. (D) Quantification of wound closure percentage over time. Data are presented as mean ± SEM ($n = 3$ biological replicates). Statistical analysis was performed using two-way ANOVA with Tukey's multiple comparisons test. * $p < 0.05$, ** $p < 0.005$, *** $p < 0.001$, ns, not significant.

RNA sequencing of SC-EVs revealed miRNA signatures in repair SC-EVs compared with immature and myelinating SC-EVs (Figure 5A). Focusing on differentially expressed miRNAs between repair and myelinating SC-EVs, we found that repair SC-EVs contain distinct miRNA signatures predicted to target neuronal compartments and repress transcripts involved in neuron projection morphogenesis, RNA biosynthesis, protein glycosylation, and myelination (Figure 5C,G,H). Pathway analysis predicted a coordinated suppression of neuronal differentiation, axon elongation and synaptic formation through PI3K/AKT, NTRK, RHO GTPase, and AP-1 signaling pathways (Figure 5I), consistent with the early repair phase's prioritization of axon outgrowth over maturation and synaptic stabilization (Lopez-Leal and Court 2016; López-Leal et al. 2020). In addition, downregulated miRNAs in repair SC-EVs were associated with de-repression of regeneration-associated genes linked to neurogenesis, neurite outgrowth, cytoskeleton remodeling, and macromolecular transport (Figure 5D), supporting structural reformation of injured axons and dendrites. Reactome pathway analysis further highlighted activation of NTRK, MAPK, and receptor tyrosine kinase pathways (Figure 5E) that support neurotrophin-mediated axon elongation and neuronal survival (Li et al. 2020). The miRNA shift may be influenced by $p75^{NTR}$ expression in repair SCs, as loss of $p75^{NTR}$ alters EV-associated small RNA profiles, including miRNAs involved in autophagy and phosphatidylinositol signaling (Gonçalves et al. 2020). These findings suggested that SC-EVs may influence gene expression during nerve injury, with their miRNA cargo contributing to both intra- and intercellular reprogramming. This aligns with prior evidence that SC-EVs promote neurite outgrowth, axonal

regrowth, and modulation of regenerative microenvironments (López-Leal et al. 2020; Xia et al. 2020), and is further supported by our transcriptomic data demonstrating that repair SCs contain distinct miRNA signatures that upregulate genes involved in axon regrowth, migration, and modulation of PI3K/Akt, ERK, and MAPK pathway modulation.

Among miRNAs identified in SC-EVs, several have established roles in promoting nerve regeneration. For example, miR-125b supports neurite elongation (Le et al. 2009), miR-138-5p inhibits apoptosis (Maza et al. 2022), and miR-193b-3p and miR-223-3p contribute to anti-inflammation (Huang et al. 2022; Lai et al. 2020). Similarly, miR-345-3p implicates in resolving inflammation and promotes neuronal survival (Wei et al. 2020). Conversely, downregulation of miR-125b, miR-140, miR-181c, and miR-199a-3p has been linked to enhanced axonal extension and cell viability (Kar et al. 2021; Kos et al. 2016; Song et al. 2024; Yuan et al. 2018), suggesting that suppression of specific miRNAs may derepress neuronal regeneration. While miR-21 is widely recognized as pro-regenerative (Cong et al. 2021; López-Leal et al. 2020), its downregulation in our dataset may reflect dynamic or stage-specific regulation during the repair process (Borger et al. 2022). Furthermore, suppression of miR-423-5p and miR-92a-2-5p, both involved with neuroprotection and neuronal differentiation (Luo et al. 2022; Zhuang et al. 2022), are consistent with transcriptional reprogramming toward a regenerative stage. Notably, several miRNAs in SC-EVs remain uncharacterized, presenting new opportunities to uncover regulatory elements underlying nerve regeneration.

In parallel, we identified highly expressed long non-coding RNAs (lncRNAs) enriched in repair SC-EVs (Figure 6), most of which are currently unannotated. Given that lncRNAs can function as molecular sponges that sequester miRNAs and relieve suppression of their target transcripts (Chen and Kim 2024; Chuang et al. 2023), we assessed potential lncRNA–miRNA interactions using miRanda (Marín and Vanícek 2011). lncRNAs exhibited strong predicted binding to miRNAs downregulated in repair SC-EVs, i.e., miR-125b, miR-149-5p, miR-222-5p, miR-330-5p, miR-503-3p, miR-423-5p, and miR-128-3p, all of which are implicated in neuroregenerative processes (Lanza et al. 2023; Li et al. 2022; Luo et al. 2022; Yuan et al. 2018; Zhou et al. 2012). These interactions demonstrated low hybridization energies and multiple binding sites, indicating stable lncRNA-miRNA complexes (Table S11). Collectively, the observations suggest that lncRNAs within SC-EVs may contribute to post-transcriptional regulation through modulation of miRNA activity during pair-associated Schwann cell responses. However, these interactions remain predictive and require further validation. In addition to miRNA sequestration, lncRNAs may also function through other mechanisms such as chromatin remodeling, transcriptional regulation, and modulation of RNA-binding proteins (Chen and Kim 2024), which warrant future investigation.

Consistent with the predicted functions of EV-associated RNAs, only repair SC-EVs induced a significant increase in SOX2 protein in immature Schwann cells (Figure 7B,C), suggesting activation of repair-associated signaling pathways. Several miRNAs identified in repair SC-EVs, such as miR-503-3p and miR-330-5p, may target upstream elements of pathways linked to SOX2 activation, including LIF/STAT3, Wnt/β-catenin, TGF-β/SMAD, and FGF/PI3K-AKT signaling (Mansouri et al. 2016; Niharika et al. 2024; Zhang et al. 2020). These findings are consistent with previous reports demonstrating that miRNAs in EVs can regulate transcriptional signaling networks and cellular reprogramming through modulation of transcription factors (Aswani et al. 2024). Functional validation of miR-330-5p provides mechanistic support for this model. miR-330-5p was among the most significantly downregulated miRNAs in repair versus myelinating SC-EVs (Figure S8), and its overexpression in RT4-D6P2T Schwann cells reduced SOX2 protein levels, decreased proliferation, and impaired wound closure, whereas its inhibition restored these effects (Figure 8). The results establish a link between miR-330-5p abundance and repair responses. In contrast, miR-503-3p produced relatively minor effects on Schwann cell proliferation and migration compared to the control, without notable effects on SOX2 expression, suggesting that individual EV-associated miRNAs may differentially contribute to repair-associated Schwann cell responses through distinct regulatory mechanisms. Future studies will be needed to further define the role and downstream targets of miR-503-3p in Schwann cells.

One limitation of this study is the use of in vitro Schwann cell models. In culture, Schwann cells lack interactions with axons, inflammatory cells, fibroblasts, extracellular matrix components, and biomechanical cues present in the nerve injury microenvironment that are known to regulate repair phenotypes and regeneration (Lu et al. 2024; Yang et al. 2025). Accordingly, the findings should be interpreted as mechanistic insights derived from a simplified in vitro system rather than a complete representation of the in vivo nerve injury microenvironment. However, this Schwann cell monoculture model provided an important advantage for mechanistic investigation of Schwann cell-derived EVs. By excluding co-secreted EVs from other injury-associated cell populations, this model enabled precise attribution of EV cargo composition and functional activity specifically to Schwann cells across distinct differentiation stages. Future studies using multicellular co-culture systems or in vivo nerve injury models will be implemented to validate these findings under physiologically relevant conditions. In addition, only a single EV dose (20 μg total EV protein; $\sim 5 \times 10^3$ EVs per cell or $\sim 5 \times 10^8$ EVs/mL) was evaluated in the functional assays. This concentration was selected based on previously reported regenerative EV dosing ranges (Wu et al. 2020). A single EV concentration was applied across all groups to enable direct comparison between stage-specific SC-EV populations. Future dose-response studies will be crucial to determine the optimal therapeutic range for SC-EV-mediated repair signaling.

Despite these limitations, our findings provide insight into the stage-dependent molecular composition of SC-EVs and support their potential role as regulators of repair-associated Schwann cell responses. Engineering strategies to enhance SC-EV production and regenerative potency represent promising avenues for translational development. Notably, mechanical and electrical stimulation of SCs has been shown to increase EV secretion and enrich their cargo with regenerative factors (Izhiman and Esfandiari 2024; Xia et al. 2020). Incorporating piezoelectric or conductive biomaterials (Bryan et al. 2023; Krutko et al. 2025; Orkwis et al. 2022; Orkwis et al. 2020; Poling et al. 2026) into culture systems may further enable stage-specific EV enrichment.

These approaches lay the groundwork for advancing SC-EVs toward translational SC-EV therapies for peripheral nerve repair.

4 | Materials and Methods

4.1 | Rat Primary Schwann Cell Culture

Primary Rat Schwann cells (RSC) (Catalog R842-05a) were purchased from CELL Applications (San Diego, CA, USA) and maintained according to the manufacturer's protocol. Briefly, Schwann cells were cultured in RSC growth medium (Catalog R825-500) (CELL Applications, San Diego, CA, USA) at 37°C in 5% CO_2. The culture medium was replaced every 48 h. Sub-culturing was performed when the cells reached 80% confluency and cells were maintained for no longer than 5 passages. Passages 3 to 5 were used for experiments.

4.2 | Rat Schwann Cell Line Culture

RT4-D6P2T rat Schwann cells (CRL-2768) were obtained from the American Type Culture Collection (ATCC, Manassas, VA, USA). Cells were cultured in Dulbecco's Modified Eagle Medium (DMEM, Corning) supplemented with 10% fetal bovine serum (FBS; Gibco), 100 U/mL penicillin, and 100 µg/mL streptomycin (Gibco). Cells were maintained at 37°C in a humidified incubator with 5% CO_2 and passaged upon reaching approximately 80% confluency.

4.3 | Cell Differentiation and Dedifferentiation Assay

Six-well plates and 11 mm glass coverslips were incubated with Schwann Cells Coating solution (Cat036-20) CELL Applications (San Diego, CA, USA) at 37°C overnight. The remaining solution was aspirated, rinsed twice with PBS, and dried. RSC samples were prepared according to a modified protocol (Zou 2023). Cells were seeded into a coated 6-well plate at a density of 2×10^5 cells/well for western blot and RNA sequencing and seeded into a 24-well plate (covered with coated glass coverslips) at a density of 1×10^4 cells/well for immunofluorescence staining. Cells were cultured in RSC complete growth medium (R825-500) for 24 h and the medium was changed into the complete medium-RSC basal media containing 10% Exosome-Depleted FBS (Gibco, Thermo Fisher Scientific, Cat# A2720801, Lot# 2631751RP; verified by the manufacturer to remove > 90% of exosome), 2 mM of Foskolin (Sigma-Aldrich, catalog number: F6886), 10 ng/mL of human neuregulin 1-β1/heregulin (R&D Systems, Catalog Number: 396-HB/CF), and 100 mg/mL penicillin-streptomycin (Gibco) for 24 h. Then the medium was removed and replaced by a medium containing DMEM, 1% Exosome-depleted FBS, and 100 mg/mL penicillin-streptomycin (starvation medium) overnight to limit mitogenic stimulation. Cells were then differentiated into myelinating SC by removing the starvation medium and replacing it with medium containing DMEM, 1% Exosome-depleted FBS, 100 mg/mL penicillin-streptomycin, and 1 mM db-cAMP (Sigma, USA). After 72 h, the medium was replaced with the Exosome-depleted complete medium for an additional 72 h to induce dedifferentiation. Cells maintained in the absence of db-cAMP-inducing agents served as a control for undifferentiated cells. Cells were monitored daily to observe changes in morphology. At the end of the assay, cells were harvested for SC stage-specific markers for characterization of Schwann cell differentiation stages, and the supernatant was collected for EV isolation.

4.4 | Immunofluorescence Staining

Cells were washed three times before fixation in 3.7% formaldehyde for 15 min at room temperature. Following two washes with PBS, cells were permeabilized with 0.1% Triton X-100 (Fisher) in PBS at 4°C for 5 min and washed with PBS. The cells were blocked with 200 uL 0.2% bovine serum albumin (BSA) in PBS (blocking buffer) for 1 h at RT, and then incubated with primary antibodies (1:400 diluted in blocking buffer) as follows; rabbit anti-p75 NGF Receptor (ab52987; Abcam, Waltham, MA, USA), rabbit anti-SOX2 (ab97959; Abcam, Waltham, MA, USA), mouse anti-c Jun (NBP2-71059, Novus Biologicals, CO, USA), rabbit anti-KROX20 (Abcam, Waltham, MA, USA) or EGR2 (ab245228; Abcam, Waltham, MA, USA) antibodies at 4°C overnight. The next day, cells were washed with PBS followed by separate incubations for 30 min at 37°C with 1:100 dilution of rhodamine phalloidin (Invitrogen, OR, UAS), goat anti-rabbit IgG Alexa Fluor 488 (ab150077; Abcam, Waltham, MA, USA), and anti-mouse IgG Alexa Fluor 647 (ab150115; Abcam Waltham, MA, USA) secondary antibodies. After washing, cells were mounted in mounting medium with DAPI (Catalog-50011, ibidi, WI, USA) on a microscope slide. Clear nail polish was used to seal coverslips. Imaging was performed using a NIKON ECIPSE TE-2000-S.

4.5 | Schwann Cell-Derived Extracellular Vesicle Isolation

EVs were isolated using an insulator-based dielectrophoretic (iDEP) as described (Sharma et al. 2023; Shi and Esfandiari 2022). The culture supernatant (5 mL) from each condition was centrifuged at 21,000×g at 4°C for 20 min to remove large EVs and cell debris. Conditioned media were concentrated 5-fold using Amicon Ultra-4 centrifugal filters (100-kDa cutoff; Millipore, Burlington, MA, USA), which also removed a substantial portion of soluble proteins prior submitted to the iDEP. Briefly, borosilicate glass capillaries (BF-100-50-15, Sutter Instrument, Novato, CA, USA) were fabricated into micropipettes with 2 µm pore diameters using a laser-assisted puller P2000 (Sutter Instrument Company, Novato, CA, USA). The micropipette was filled with 0.02-µm filtered 1x PBS buffer using a 33-gauge Hamilton syringe needle and positioned on a substrate. Then, 1X filtered PBS and 50 µL of sample were loaded at the base side and tip side of the micropipette, respectively. EVs were trapped at the tip by applying a 10 V/cm direct current (DC) for 15 min, followed by a release in 15 µL 1× filtered PBS by reversing the applied voltage for another 10 min. Isolated EVs were aliquoted and stored at −80°C for further analysis. Only one freeze-thaw cycle was allowed for each aliquot.

4.6 | Western Blot Analysis

Cell and EV samples were lysed in 1X RIPA buffer (Abcam) and 1X protease/phosphatase inhibitor (Abcam). The samples were subjected to measure protein concentration using the DC Protein Assay (Bio-Rad, Hercules, CA, USA. For validation of Schwann cell molecular markers, 5 μg of total cellular protein was loaded per lane. For EV marker analysis, 1 μg of total protein from both EVs and corresponding cell lysates was loaded to enable direct comparison of marker enrichment between cellular and EV fractions. Samples were mixed with 4x Laemmli buffer (Bio-Rad), heated at 95°C for 5 mins. The samples were run into a 4–20% Mini-PROTEAN TGX Precast Protein gel, 200 V for 35 min before being transferred onto a PVDF membrane using a Trans-Blot Turbo System (Bio-Rad). The membrane was blocked with EveryBlot blocking buffer (Biorad) for 5 min, and then probed with 1:1,000 dilution of primary antibodies as follows; rabbit anti-p75 NGF Receptor (ab52987; Abcam, Waltham, MA, USA), rabbit anti-SOX2 (ab97959; Abcam), rabbit anti-c Jun (ab40766; Abcam), rabbit anti-KROX20 or EGR2 (ab245228; Abcam) and human anti- myelin basic protein (ab209328; Abcam) antibodies for SC markers, mouse anti-beta actin antibody (Ab6276; Abcam), and mouse anti-CD63 (Ab108950; Abcam), rabbit anti-TSG101 (ab125011;Abcam) and rabbit anti-HSP70 (ab181606; Abcam) antibodies for EV common markers at 4°C overnight. After washing, the membranes were incubated with secondary antibody specific to the species of the primary antibody at a dilution of 1:2000 as follows; goat anti-rabbit IgG-HRP, goat anti-mouse IgG-HRP (Abcam), and goat anti-human IgG-HRP (Abcam) at room temperature for 1 h. The immunoblot was developed by ECL (Bio-Rad, USA) for the cell samples and SuperSignal West Pico PLUS (Thermo) for the EV samples. The membrane was imaged on a ChemiDoc MP imaging system (Bio-Rad, USA). Signal intensities were quantified using the Image J software (NIH, USA). At least three independent experiments were performed. For SCs, protein bands were normalized to actin and quantified relative to the control (undifferentiated condition). For EVs, band intensities were quantified relative to the control (undifferentiated condition).

4.7 | Nanoparticle Tracking Analysis (NTA)

A NanoSight NS300 (Malvern Instruments Ltd., Malvern, Worcestershire, UK), integrated with a sample pump, was utilized for the analysis. EV samples were diluted in 0.22 μm filtered 1x PBS at a ratio of 1:40 to achieve a total volume of 1 mL. The diluted sample was then injected into the sample chamber using the syringe pump. Five 1-minute videos were recorded under the following parameters: camera: sCMOS; cell temperature: 25°C; syringe pump speed: 30 μL/s. After capture, the videos were analysed by NanoSight Software NTA 3.4 Build 3.4.003 using the settings: detection threshold, 5; blur size and max jump distance, auto. Ideal concentrations contained 20–100 particles/frame.

4.8 | Transmission Electron Microscopy (TEM)

TEM was performed to visualize the morphology of SC-EVs. Five microliters of isolated EVs were applied onto 200-mesh carbon-coated copper grids (FCF200-CU; Electron Microscopy Sciences) and allowed to adsorb for approximately 1 min at room temperature. The grids were gently rinsed twice with deionized water and subsequently stained with 2% uranyl acetate (Cat# 22400; Electron Microscopy Sciences) for 10 s. After removing excess stain with filter paper, grids were air-dried for 1 min. Imaging was performed on a Thermo Talos L120C transmission electron microscope operated at 100 kV.

4.9 | Super-Resolution Microscopy

Single-level EV images were obtained using a Nano imager S Mark II microscope (Oxford Nanoimaging, Oxford, UK) equipped with a 100X, 1.4 NA oil immersion objective, an XYZ closed-loop piezo 736 stage, and dual or triple emission channels split at 640 and 555 nm. EV samples were prepared according to a modified protocol (Wiklander et al. 2024). 1×10^9 EVs were stained with 5ug of primary antibodies in combination of mouse anti-CD63 (Ab108950; abcam) and rabbit anti-p75 NGF Receptor (ab52987; abcam) in 100 μL 0.2% BSA in PBS overnight on a shaker at 4°C. Next day, samples were wash with 400 μL filtered 1xPBS for three times using Ultracel-100 K membrane filter (Merck Millipore, Burlington, MA, USA) at 5000 RPM for 3 min. Samples were collected and labeled with secondary antibodies including Goat pAb to mouse IgG AF488 (AB150116) and Goat pAb to rabbit IgG AF594 (Abcam, Waltham, MA, USA) at a dilution of 1:400 in 400 μL 0.2% BSA in PBS for 3 h at 4°C. Following reaction completion, samples were washed three times with filtered 1X PBS and collected in a final volume of 100 μL. For imaging, μ-Slide 8 well glass bottom slides (Ibidi, Fitchburg, WI, USA) were washed two times with distilled water, coated with 100 uL poly-L-lysine solution (Sigma Aldrich, St. Louis, MO, USA), and incubated at 37°C overnight. Upon incubation, the solution was carefully removed and the sample of antibodies-EVs was added at a final volume of 100 μL and kept at 4°C overnight. The next day, the buffer was removed, washed, and fixed with 3.7% formaldehyde for 15 min at 4°C. Lastly, samples were washed 3X with filtered PBS. Three to five fields of view were recorded for each sample using direct stochastical optical reconstruction microscopy (dSTORM). Analysis was performed using algorithms including filtering, drift correction, and DBScan clustering developed by ONI (Oxford Nanoimaging, Oxford, UK) via the Collaborative Discovery (CODI) platform. The dSTORM analysis was performed qualitatively to visualize the co-localization and expression of CD63 and p75NTR on individual EVs.

4.10 | Whole RNA Sequencing for mRNA and lncRNA

Whole-transcriptome RNA sequencing was performed by the Genomics, Epigenomics, and Sequencing Core (GESC) at the University of Cincinnati following updated protocols as previously described (Qiu et al. 2023; Reigle et al. 2021). Total RNA was isolated from Schwann cells for mRNA-seq and SC-EVs for lncRNA-seq, and quality control was assessed using the Agilent Bioanalyzer with the RNA 6000 Pico Kit (Agilent Technologies, Santa Clara, CA). Gel-like images and electropherograms of total RNA from Schwann cells and SC-EVs demonstrated distinct 28S and 18S rRNA peaks and RNA fragment distributions above 200 nt, confirming good RNA quality suitable for mRNA and lncRNA sequencing (Figures S3 and S7). Next, 10 ng of total RNA

was used as input for library preparation using the NEBNext Ultra II Directional RNA Library Prep Kit (New England BioLabs, Ipswich, MA). PCR was run for 9 cycles. Library quality and concentration were evaluated using Qubit fluorometric quantification (Thermo Fisher Scientific, Waltham, MA). Each library was then uniquely indexed and proportionally pooled. The final library pool was sequenced on the Illumina NextSeq 2000 platform (Illumina, San Diego, CA) with setting of PE 2×61 bp to generate ∼30 million reads per sample for mRNA and ∼20 million reads per sample for lncRNA. Sequencing output was processed via the Illumina BaseSpace Sequence Hub to generate fastq files for downstream mRNA and long noncoding RNA (lncRNA) analysis.

4.11 | MicroRNA-Sequencing

Small RNA sequencing was carried out by the GESC following established protocols (Langevin et al. 2020; Sheth et al. 2025). Total RNA isolated from SC-EVs was quantified and quality control-assessed using the RNA 6000 Pico Kit on the Agilent Bioanalyzer (Agilent Technologies, Santa Clara, CA). Gel-like images and electropherograms revealed RNA fragments below 200 nucleotides, corresponding to small RNAs, confirming good RNA quality suitable for miRNA sequencing (Figure S7). ∼5 ng of total RNA was used for library construction with the NEBNext Multiplex Small RNA Library Prep Kit (New England BioLabs, Ipswich, MA), incorporating a protocol modification to increase sensitivity and specificity for small RNA detection. PCR amplification was performed with 15 cycles, and 10 µL of each uniquely indexed PCR mixture was pooled. The pooled libraries were then subjected to DNA purification using the DNA Clean & Concentrator kit (Zymo Research, Irvine, CA). For precise size selection, the libraries were spiked with custom 135 and 146 bp DNA ladders and run on a high-resolution agarose gel electrophoresis. MiRNA-containing fragments, ranging from 135 to 146 bp (including adapters and miRNA inserts), were cut, gel-purified, and quantified using the NEBNext Library Quantification Kit on a QuantStudio 5 Real-Time PCR System (Thermo Scientific). Quantified libraries were low-depth sequenced on the Illumina NextSeq 2000 platform (Illumina, San Diego, CA) for the first round to generate a few million reads per sample. Based on the preliminary read counts, library input volumes were adjusted to normalize sample representation. A second round, high-depth sequencing run was subsequently performed to generate ∼40 million reads per sample for final data analysis.

4.12 | Bioinformatics and Data Analysis

4.12.1 | MRNA Analysis

RNA sequencing reads in FASTQ format were first subsampled, and strandedness was inferred using fq tool (https://github.com/stjude-rust-labs/fq). Quality control was performed with FastQC (http://www.bioinformatics.babraham.ac.uk/projects/fastqc), followed by adapter and quality trimming using Trim Galore (https://www.bioinformatics.babraham.ac.uk/projects/trim_galore) and Cutadapt (Martin 2011). Sequencing quality controls including total reads, duplication rates, and GC content were evaluated using FastQC and summarized with MultiQC, confirming consistently high per-base quality scores (Figure S9). Trimmed reads were aligned to the rat reference genome using the STAR (Dobin et al. 2013), with HISAT2 (Kim et al. 2019) as an alternative aligner. The alignments were sorted and indexed using SAMtools (Li et al. 2009), and PCR duplicates were marked using Picard MarkDuplicates (http://broadinstitute.github.io/picard/). Transcript assembly and quantification were performed using StringTie (Pertea et al. 2015). BEDTools (Quinlan and Hall 2010) and bedGraphToBigWig were used to generate bigWig tracks. Intensive quality control of the RNA-seq data was carried out using tools including RSeQC (Wang et al. 2012), Qualimap (Okonechnikov et al. 2016), and dupRadar (Sayols et al. 2016). Transcript quantification was performed using Salmon (Patro et al. 2017), and transcript counts were converted to gene counts using the tximport package (https://github.com/thelovelab/tximport). Differential gene expression analysis between sample groups was conducted using DESeq2 v1.26.0 (Love et al. 2014). Only read count sum > 30 were included for differential-expression analysis. Hierarchical clustering heatmaps of differentially expressed genes (DEGs: $\log_2$ fold change ≥ |0.58| and q-value ≤ 0.05) were generated. Genes with $\log_2$ fold change ≥ 1.5 or ≤ -1.5 and q-value ≤ 0.05 were considered significantly differentially expressed and visualized in volcano plots. All upregulated genes were submitted to DAVID (http://david.ncifcrf.gov) for gene ontology (GO) enrichment analysis (Huang da et al. 2009; Sherman et al. 2022) to identify the top 10 biological processes ranked by fold enrichment (FDR < 0.05). Additionally, genes ranked by $\log_2$ fold change were submitted for gene set enrichment analysis (GSEA) using the GSEA tool (Subramanian et al. 2005). Gene sets upregulated in the "na_pos" phenotype with FDR < 25% were considered significant. All visualization were generated using SRplot (Tang et al. 2023).

4.12.2 | MiRNA Analysis

miRNA sequencing data were processed using the nf-core/smrnaseq pipeline (version 2.3.1), which performs adapter trimming, quality control, alignment, and quantification of small RNA reads. The pipeline generated both raw and normalized gene count files, with normalization reported in counts per million. A summary report of quality control metrics and pipeline outputs was generated using MultiQC (Ewels et al. 2016). Sequencing QC parameters, including total reads, GC content, and duplication rates, were evaluated using FastQC and MultiQC, confirming high-quality reads suitable for downstream analysis (Figure S10). Differential expression analysis between sample groups was conducted using the DESeq2 package (v1.26.0) in R (Love et al. 2014). For downstream analysis, read count sum > 30 were included for differential-expression analysis. Significantly differentially expressed miRNAs were identified based on $\log_2$FoldChange ≥ |0.58| and false discovery rate (FDR) ≤ 0.05. DEGs clustering heatmaps were generated using SRplot (Tang et al. 2023), and the two primary clusters representing upregulated and downregulated miRNAs in myelinating versus repair SC-EV groups were selected for downstream analysis. Target prediction for differentially expressed miRNAs was performed using the intersection of miRWalk (version 3.0, binding P-value ≥ 0.95) (Sticht et al. 2018) and miRDB

(prediction score >50) (Chen and Wang 2020). Predicted target genes were submitted to DAVID (http://david.ncifcrf.gov) for gene ontology (GO) analysis to identify the top 10 cellular compartments. The DAVID gene functional classification tool (http://david.ncifcrf.gov) (Huang et al. 2007) was used to identify four functional clusters ranked by enrichment score (P-value ≤ 0.05). All visualizations were performed using SRplot (Tang et al. 2023).

4.12.3 | LncRNA Analysis

RNA sequencing reads were assessed for quality using FastQC (https://github.com/stjude-rust-labs/fq) (Figure S11) and subsequently trimmed to remove adapter sequences using Trim Galore (https://www.bioinformatics.babraham.ac.uk/projects/trim_galore) and Cutadapt (Martin 2011). The cleaned reads were aligned to the rat reference genome using the STAR aligner (Dobin et al. 2013). Raw counts and lncRNA expression (Transcripts Per Million, TPM) were generated. The top 20 most highly expressed lncRNAs were used to generate heatmap. Upregulated clusters from the heatmap were subjected to miRNA-lncRNA interaction prediction using miRanda through SRplot (Tang et al. 2023). Interactions with high binding affinity (total score >140 and minimum free energy < −20 kcal/mol) were selected (Marín and Vanícek 2011). All data visualization and plotting were performed using SRplot (Tang et al. 2023).

4.13 | Quantification of miRNA Expression by qRT-PCR

miRNA expression was quantified using the miRCURY LNA SYBR Green system (QIAGEN). Total RNA (~0.3 ng per 10 µL RT reaction) was reverse transcribed into cDNA with the miRCURY LNA RT Kit (QIAGEN, Cat. No. 339340) including the UniSp6 RNA spike-in as an exogenous control. The cDNA was diluted 1:30 and amplified using the miRCURY LNA SYBR Green PCR Kit (QIAGEN, Cat. No. 339345) with target-specific primers for rno-miR-503-3p and rno-miR-330-5p (Primer assay, QIAGEN, Cat. No. 339306). Each 10 µL PCR reaction contained 5 µL of 2× SYBR Green Master Mix, 1 µL of primer assay, 1 µL of nuclease-free water, and 3 µL of diluted cDNA. Amplification was performed in StepOne Real-Time PCR System (Applied Biosystems) using the following cycling conditions: 95°C for 2 min, followed by 60 cycles of 95°C for 10 s and 56°C for 60 s, with a melt-curve analysis. Non-template controls (NTCs) were included as a negative control. Relative expression levels were determined using the ΔΔCt method, normalized to U6 snRNA, with immature SC-EVs serving as the comparator group.

4.14 | SC-EV Treatment and SOX2 Expression Analysis

Primary immature Schwann cells were plated in 12-well plates and cultured in growth medium containing EV-depleted FBS for 24 h before treatment. Cells were then treated with immature, myelinating, or repair SC-EVs at 20 µg total EV protein (quantified by DC Protein assay), equivalent to 5×10^3 EVs per recipient cell for 72 h at 37°C in a humidified 5% CO_2 atmosphere before SOX2 analysis by western blotting. Medium alone was served as a control. All treatments were conducted with three biological replicates per group.

4.15 | MiR-330-5p and miR-503-3p Mimic/Inhibitor Transfection

RT4-D6P2T rat Schwann cells were seeded in 24-well plates for Western blot analysis and 96-well plates for MTT assays and cultured in complete growth medium until approximately 60–70% confluency. Cells were then transfected with 5 nM rno-miR-330-5p miRCURY LNA miRNA Mimic (GeneGlobe ID: YM00472899-ADB), rno-miR-503-3p miRCURY LNA miRNA Mimic (GeneGlobe ID: YM00471651-ADB), Negative Control miRCURY LNA miRNA Mimic (GeneGlobe ID: YM00479902-ADB), rno-miR-330-5p miRCURY LNA miRNA Inhibitor (GeneGlobe ID: YI04101483-DDA), rno-miR-503-3p miRCURY LNA miRNA Inhibitor (GeneGlobe ID: YI04107715-DDA), or Negative Control A miRCURY LNA miRNA Inhibitor (GeneGlobe ID: YI00199006-DDA) (QIAGEN, MD, USA) using Lipofectamine RNAiMAX Transfection Reagent (Invitrogen, Thermo Fisher Scientific) according to the manufacturer's instructions.

Transfection complexes were prepared in Opti-MEM reduced-serum medium (Gibco) and added to the cells. Following transfection, cells were incubated for 96 h at 37°C in a humidified atmosphere containing 5% CO_2 prior to downstream analyses. SOX2 protein expression was evaluated by western blotting, and cell proliferation was assessed using the MTT assay.

4.16 | MTT Cell Proliferation Assay

Cell proliferation was evaluated using the CyQUANT MTT Cell Viability Assay Kit (Invitrogen, Waltham, MA, USA) according to the manufacturer's protocols. Following 96 h post-transfection, culture medium was replaced with 100 µL of culture medium containing 10 µL of 12 mM MTT stock solution. Cells were incubated for 2 h at 37°C in a humidified incubator with 5% CO_2. After incubation, the supernatant was carefully removed, and 50 µL of dimethyl sulfoxide (DMSO) was added to dissolve the formazan crystals. The plate was incubated for an additional 10 min at room temperature. Absorbance was measured at 540 nm using a BioTek 800 TS microplate reader (Agilent, Santa Clara, CA, USA). Cell proliferation was normalized to the negative control group and presented as percentage relative to negative control conditions.

4.17 | Wound Healing and Migration Assays

Schwann cells were reverse-transfected with miRNA mimics or inhibitors using Lipofectamine RNAiMAX Transfection Reagent (Invitrogen, Thermo Fisher Scientific) and seeded into 2-well adhesive silicone inserts (ibidi, Germany) placed in 24-well plates for 48 h. Following incubation, the inserts were carefully removed to generate a uniform cell-free gap of approximately 500 µm between cell populations. Fresh culture medium was then added, and phase-contrast images were acquired at 0 h, 12 h, and 24 h using a NIKON ECIPSE TE-2000-S microscope. Wound closure

area was quantified using ImageJ software (NIH, USA) together with the ImageJ plugin for in vitro scratch wound healing assays (Suarez-Arnedo et al. 2020). Results were expressed as percentage of wound closure relative to the initial wound area at 0 h. Three independent biological replicates were analyzed for each condition.

Author Contributions

Manju Sharma: writing – review and editing, methodology, investigation. **Supasek Kongsomros**: conceptualization, methodology, investigation, visualization, writing – original draft, writing – review and editing. **Maulee Sheth**: methodology, investigation, writing – review and editing. **Somchai Chutipongtanate**: investigation, writing – review and editing. **Leyla Esfandiari**: conceptualization, writing – review and editing, funding acquisition, supervision.

Acknowledgements

This study was made successful through the support and collaboration of several core facilities and individuals. RNA isolation and sequencing were performed by the Genomics, Epigenomics, and Sequencing Core (GESC) at the University of Cincinnati. We gratefully acknowledge Xiang Zhang and Sam Bell from GESC, and the team at Information Services for Research (IS4R), Cincinnati Children's Hospital Medical Center: Aditi Paranje, Ronika De, and Ashley Kuenzi for their invaluable bioinformatics expertise and technical support, which significantly contributed to the success of this work. We also sincerely thank Dr. Desirée Benefield at the Center for Advanced Structural Biology (CASB) for her expert assistance and guidance with transmission electron microscopy (TEM) imaging. Graphical abstract and Figure 1A were created with BioRender.com.

Funding

This work was supported by the National Institute of General Medical Sciences of the National Institutes of Health under award number 1R35GM150860-01.

Conflicts of Interest

The authors have no conflicts of interest to declare.

Data Availability Statement

The data that support the findings of this study have been deposited in the NCBI Gene Expression Omnibus (GEO) under accession number GSE300703 and are publicly available at: https://www.ncbi.nlm.nih.gov/geo/query/acc.cgi?acc = GSE300703.

References

Aswani, B. S., M. Hegde, R. Vishwa, et al. 2024. "Tackling Exosome and Nuclear Receptor Interaction: An Emerging Paradigm in the Treatment of Chronic Diseases." *Military Medical Research* 11, no. 1: 67. https://doi.org/10.1186/s40779-024-00564-1.

Balakrishnan, A., M. G. Stykel, Y. Touahri, J. A. Stratton, J. Biernaskie, and C. Schuurmans. 2016. "Temporal Analysis of Gene Expression in the Murine Schwann Cell Lineage and the Acutely Injured Postnatal Nerve." *PLoS ONE* 11, no. 4: e0153256. https://doi.org/10.1371/journal.pone.0153256.

Benito, C., C. M. Davis, J. A. Gomez-Sanchez, et al. 2017. "STAT3 Controls the Long-Term Survival and Phenotype of Repair Schwann Cells During Nerve Regeneration." *Journal of Neuroscience* 37, no. 16: 4255–4269. https://doi.org/10.1523/jneurosci.3481-16.2017.

Boerboom, A., V. Dion, A. Chariot, and R. Franzen. 2017. "Molecular Mechanisms Involved in Schwann Cell Plasticity." *Frontiers in Molecular Neuroscience* 10: 38. https://doi.org/10.3389/fnmol.2017.00038.

Borger, A., S. Stadlmayr, M. Haertinger, et al. 2022. "How miRNAs Regulate Schwann Cells During Peripheral Nerve Regeneration-A Systemic Review." *International Journal of Molecular Sciences* 23, no. 7: 3440. https://doi.org/10.3390/ijms23073440.

Bosch-Queralt, M., R. Fledrich, and R. M. Stassart. 2023. "Schwann Cell Functions in Peripheral Nerve Development and Repair." *Neurobiology of Disease* 176: 105952. https://doi.org/10.1016/j.nbd.2022.105952.

Bryan, A. E., M. Krutko, J. Westphal, M. Sheth, L. Esfandiari, and G. M. Harris. 2023. "Ultrasound-Activated Piezoelectric Polyvinylidene Fluoride–Trifluoroethylene Scaffolds for Tissue Engineering Applications." *Military Medicine* 188, no. 6: 61–66. https://doi.org/10.1093/milmed/usad018.

Chen, L. L., and V. N. Kim. 2024. "Small and Long Non-coding RNAs: Past, Present, and Future." *Cell* 187, no. 23: 6451–6485. https://doi.org/10.1016/j.cell.2024.10.024.

Chen, S. H., C. C. Wu, W. L. Tseng, et al. 2023. "Adipose-derived Stem Cells Modulate Neuroinflammation and Improve Functional Recovery in Chronic Constriction Injury of the Rat Sciatic Nerve." *Frontiers in neuroscience* 17: 1172740. https://doi.org/10.3389/fnins.2023.1172740.

Chen, T. Y., E. Gonzalez-Kozlova, T. Soleymani, et al. 2022. "Extracellular Vesicles Carry Distinct Proteo-transcriptomic Signatures That Are Different From Their Cancer Cell of Origin." *Iscience* 25, no. 6: 104414. https://doi.org/10.1016/j.isci.2022.104414.

Chen, W., S. Chang, C. Yang, et al. 2022. "Schwann Cell-Like Cells Derived From human Amniotic Mesenchymal Stem Cells Promote Sciatic Nerve Repair Through an Exosome-Induced SOX2/FN1 Pathway in Vitro." *International Journal of Molecular Medicine* 49, no. 6: 80. https://doi.org/10.3892/ijmm.2022.5136.

Chen, Y., and X. Wang. 2020. "miRDB: An Online Database for Prediction of Functional microRNA Targets." *Nucleic acids research* 48, no. D1: D127–D131.

Chuang, Y. T., J. P. Shiau, J. Y. Tang, et al. 2023. "Connection of Cancer Exosomal LncRNAs, Sponging miRNAs, and Exosomal Processing and Their Potential Modulation by Natural Products." *Cancers (Basel)* 15, no. 8: 2215. https://doi.org/10.3390/cancers15082215.

Chutipongtanate, S., S. Kongsomros, N. Pongsakul, et al. 2022. "Anti-SARS-CoV-2 Effect of Extracellular Vesicles Released From Mesenchymal Stem Cells." *Journal of Extracellular Vesicles* 11, no. 3: e12201. https://doi.org/10.1002/jev2.12201.

Conesa, A., P. Madrigal, S. Tarazona, et al. 2016. "A Survey of Best Practices for RNA-seq Data Analysis." *Genome Biology* 17, no. 1: 13. https://doi.org/10.1186/s13059-016-0881-8.

Cong, M., M. Shen, X. Wu, et al. 2021. "Improvement of Sensory Neuron Growth and Survival via Negatively Regulating PTEN by miR-21-5p-contained Small Extracellular Vesicles From Skin Precursor-derived Schwann Cells." *Stem Cell Res Ther* 12, no. 1: 80. https://doi.org/10.1186/s13287-020-02125-4.

Daboussi, L., G. Costaguta, M. Gullo, et al. 2023. "Mitf Is a Schwann Cell Sensor of Axonal Integrity That Drives Nerve Repair." *Cell reports* 42, no. 11: 113282. https://doi.org/10.1016/j.celrep.2023.113282.

Dixson, A. C., T. R. Dawson, D. Di Vizio, and A. M. Weaver. 2023. "Context-specific Regulation of Extracellular Vesicle Biogenesis and Cargo Selection." *Nature Reviews Molecular Cell Biology* 24, no. 7: 454–476. https://doi.org/10.1038/s41580-023-00576-0.

Dobin, A., C. A. Davis, F. Schlesinger, et al. 2013. "STAR: Ultrafast Universal RNA-seq Aligner." *Bioinformatics* 29, no. 1: 15–21.

Ewels, P., M. Magnusson, S. Lundin, and M. Käller. 2016. "MultiQC: Summarize Analysis Results for Multiple Tools and Samples in a Single Report." *Bioinformatics* 32, no. 19: 3047–3048. https://doi.org/10.1093/bioinformatics/btw354.

Feltri, M. L., Y. Poitelon, and S. C. Previtali. 2016. "How Schwann Cells Sort Axons: New Concepts." *The Neuroscientist* 22, no. 3: 252–265. https://doi.org/10.1177/1073858415572361.

Follis, R. M., C. Tep, T. C. Genaro-Mattos, et al. 2021. "Metabolic Control of Sensory Neuron Survival by the p75 Neurotrophin Receptor in Schwann Cells." *Journal of Neuroscience* 41, no. 42: 8710–8724. https://doi.org/10.1523/jneurosci.3243-20.2021.

Gonçalves, N. P., Y. Yan, M. Ulrichsen, et al. 2020. "Modulation of Small RNA Signatures in Schwann-Cell-Derived Extracellular Vesicles by the p75 Neurotrophin Receptor and Sortilin." *Biomedicines* 8, no. 11: 450. https://doi.org/10.3390/biomedicines8110450.

Gonias, S. L., and W. M. Campana. 2023. "Schwann Cell Extracellular Vesicles: Judging a Book by Its Cover." *Neural Regen Res* 18, no. 2: 325–326. https://doi.org/10.4103/1673-5374.346478.

Huang, B., S. Guo, Y. Zhang, et al. 2022. "MiR-223-3p Alleviates Trigeminal Neuropathic Pain in the Male Mouse by Targeting MKNK2 and MAPK/ERK Signaling." *Brain Behav* 12, no. 7: e2634. https://doi.org/10.1002/brb3.2634.

Huang, D. W., B. T. Sherman, Q. Tan, et al. 2007. "The DAVID Gene Functional Classification Tool: A Novel Biological Module-Centric Algorithm to Functionally Analyze Large Gene Lists." *Genome Biology* 8: 1–16.

da Huang, W., B. T. Sherman, and R. A. Lempicki. 2009. "Systematic and Integrative Analysis of Large Gene Lists Using DAVID Bioinformatics Resources." *Nature Protocols* 4, no. 1: 44–57. https://doi.org/10.1038/nprot.2008.211.

Izhiman, Y., and L. Esfandiari. 2024. "Emerging Role of Extracellular Vesicles and Exogenous Stimuli in Molecular Mechanisms of Peripheral Nerve Regeneration." *Front Cell Neurosci* 18: 1368630. https://doi.org/10.3389/fncel.2024.1368630.

Jessen, K. R., and R. Mirsky. 2021. "The Role of c-Jun and Autocrine Signaling Loops in the Control of Repair Schwann Cells and Regeneration." *Front Cell Neurosci* 15: 820216. https://doi.org/10.3389/fncel.2021.820216.

Jessen, K. R., and R. Mirsky. 2022. "Schwann Cells in Nerve Repair and regeneration." In *Peripheral Nerve Tissue Engineering and Regeneration*, (385–401). Springer.

Kar, A. N., S. J. Lee, P. K. Sahoo, et al. 2021. "MicroRNAs 21 and 199a-3p Regulate Axon Growth Potential Through Modulation of Pten and mTor mRNAs." *eNeuro* 8, no. 4: ENEURO.0155–0121.2021. https://doi.org/10.1523/eneuro.0155-21.2021.

Kim, D., J. M. Paggi, C. Park, C. Bennett, and S. L. Salzberg. 2019. "Graph-based Genome Alignment and Genotyping With HISAT2 and HISAT-genotype." *Nature Biotechnology* 37, no. 8: 907–915. https://doi.org/10.1038/s41587-019-0201-4.

Kongsomros, S., N. Pongsakul, J. Panachan, et al. 2022. "Comparison of Viral Inactivation Methods on the Characteristics of Extracellular Vesicles From SARS-CoV-2 Infected human Lung Epithelial Cells." *Journal of Extracellular Vesicles* 11, no. 12: e12291. https://doi.org/10.1002/jev2.12291.

Kos, A., N. Olde Loohuis, J. Meinhardt, et al. 2016. "MicroRNA-181 Promotes Synaptogenesis and Attenuates Axonal Outgrowth in Cortical Neurons." *Cellular and Molecular Life Sciences* 73, no. 18: 3555–3567. https://doi.org/10.1007/s00018-016-2179-0.

Krutko, M., H. M. Poling, M. Sheth, et al. 2025. "Thermal Annealing Enhances Piezoelectricity and Regenerative Potential of PVDF-TrFE Nanofiber Scaffolds." *Adv Mater Technol* 10: e01513. https://doi.org/10.1002/admt.202401513.

Lai, N., D. Wu, T. Liang, et al. 2020. "Systemic Exosomal miR-193b-3p Delivery Attenuates Neuroinflammation in Early Brain Injury After Subarachnoid Hemorrhage in Mice." *Journal of Neuroinflammation* 17, no. 1: 74. https://doi.org/10.1186/s12974-020-01745-0.

Langevin, S. M., D. Kuhnell, J. Biesiada, et al. 2020. "Comparability of the Small RNA Secretome Across human Biofluids Concomitantly Collected From Healthy Adults." *PLoS ONE* 15, no. 4: e0229976. https://doi.org/10.1371/journal.pone.0229976.

Lanza, M., S. Cuzzocrea, S. Oddo, E. Esposito, and G. Casili. 2023. "The Role of miR-128 in Neurodegenerative Diseases." *International Journal of Molecular Sciences* 24, no. 7: 6024. https://doi.org/10.3390/ijms24076024.

Le, M. T., H. Xie, B. Zhou, et al. 2009. "MicroRNA-125b Promotes Neuronal Differentiation in human Cells by Repressing Multiple Targets." *Molecular and Cellular Biology* 29, no. 19: 5290–5305. https://doi.org/10.1128/mcb.01694-08.

Leitman, E. M., A. Tewari, M. Horn, et al. 2011. "MLCK Regulates Schwann Cell Cytoskeletal Organization, Differentiation and Myelination." *Journal of Cell Science* 124, no. Pt 22: 3784–3796. https://doi.org/10.1242/jcs.080200.

Li, H., B. Handsaker, A. Wysoker, et al. 2009. "The Sequence Alignment/Map Format and SAMtools." *Bioinformatics* 25, no. 16: 2078–2079. https://doi.org/10.1093/bioinformatics/btp352.

Li, M., M. C. Banton, Q. Min, D. B. Parkinson, and X. Dun. 2021. "Meta-Analysis Reveals Transcription Factor Upregulation in Cells of Injured Mouse Sciatic Nerve." *Front Cell Neurosci* 15: 688243. https://doi.org/10.3389/fncel.2021.688243.

Li, R., D. H. Li, H. Y. Zhang, J. Wang, X. K. Li, and J. Xiao. 2020. "Growth Factors-based Therapeutic Strategies and Their Underlying Signaling Mechanisms for Peripheral Nerve Regeneration." *Acta Pharmacologica Sinica* 41, no. 10: 1289–1300. https://doi.org/10.1038/s41401-019-0338-1.

Li, Y., M. Sun, X. Wang, et al. 2022. "Dental Stem Cell-derived Extracellular Vesicles Transfer miR-330-5p to Treat Traumatic Brain Injury by Regulating Microglia Polarization." *Int J Oral Sci* 14, no. 1: 44. https://doi.org/10.1038/s41368-022-00191-3.

Liu, Z., Y. Q. Jin, L. Chen, et al. 2015. "Specific Marker Expression and Cell state of Schwann Cells During Culture in Vitro." *PLoS ONE* 10, no. 4: e0123278. https://doi.org/10.1371/journal.pone.0123278.

Lopez-Leal, R., and F. A. Court. 2016. "Schwann Cell Exosomes Mediate Neuron-Glia Communication and Enhance Axonal Regeneration." *Cellular and Molecular Neurobiology* 36, no. 3: 429–436. https://doi.org/10.1007/s10571-015-0314-3.

López-Leal, R., F. Díaz-Viraqué, R. J. Catalán, et al. 2020. "Schwann Cell Reprogramming Into Repair Cells Increases miRNA-21 Expression in Exosomes Promoting Axonal Growth." *Journal of Cell Science* 133, no. 12: jcs239004. https://doi.org/10.1242/jcs.239004.

Lopez-Verrilli, M. A., F. Picou, and F. A. Court. 2013. "Schwann Cell-derived Exosomes Enhance Axonal Regeneration in the Peripheral Nervous System." *Glia* 61, no. 11: 1795–1806. https://doi.org/10.1002/glia.22558.

Love, M. I., W. Huber, and S. Anders. 2014. "Moderated Estimation of Fold Change and Dispersion for RNA-seq Data With DESeq2." *Genome Biology* 15: 1–21.

Lu, P., Z. Chen, M. Wu, et al. 2024. "Type I Collagen Extracellular Matrix Facilitates Nerve Regeneration via the Construction of a Favourable Microenvironment." *Burns Trauma* 12: tkae049. https://doi.org/10.1093/burnst/tkae049.

Luo, J., N. Jiang, J. Chen, et al. 2022. "Inhibition of miR-423-5p Exerts Neuroprotective Effects in an Experimental Rat Model of Cerebral Ischemia/Reperfusion Injury." *Neuroscience* 503: 95–106. https://doi.org/10.1016/j.neuroscience.2022.08.024.

Luo, L., Y. He, X. Wang, et al. 2018. "Potential Roles of Dental Pulp Stem Cells in Neural Regeneration and Repair." *Stem Cells Int* 2018: 1731289. https://doi.org/10.1155/2018/1731289.

M, H. R., E. Bayraktar, K. H. G, et al. 2017. "Exosomes: From Garbage Bins to Promising Therapeutic Targets." *International Journal of Molecular Sciences* 18, no. 3: 538. https://doi.org/10.3390/ijms18030538.

Mansouri, S., R. Nejad, M. Karabork, et al. 2016. "Sox2: regulation of Expression and Contribution to Brain Tumors." *CNS Oncol* 5, no. 3: 159–173. https://doi.org/10.2217/cns-2016-0001.

Marín, R. M., and J. Vanícek. 2011. "Efficient Use of Accessibility in microRNA Target Prediction." *Nucleic Acids Research* 39, no. 1: 19–29. https://doi.org/10.1093/nar/gkq768.

Martin, M. 2011. "Cutadapt Removes Adapter Sequences From High-throughput Sequencing Reads." *EMBnet journal* 17, no. 1: 10–12.

Martini, R., S. Fischer, R. López-Vales, and S. David. 2008. "Interactions Between Schwann Cells and Macrophages in Injury and Inherited Demyelinating Disease." *Glia* 56, no. 14: 1566–1577. https://doi.org/10.1002/glia.20766.

Maza, R. M., M. A. Barreda-Manso, D. Reigada, et al. 2022. "MicroRNA-138-5p Targets Pro-Apoptotic Factors and Favors Neural Cell Survival: Analysis in the Injured Spinal Cord." *Biomedicines* 10, no. 7: 1559. https://doi.org/10.3390/biomedicines10071559.

Monje, P. V. 2018. "Scalable Differentiation and Dedifferentiation Assays Using Neuron-Free Schwann Cell Cultures." *Methods in Molecular Biology* 1739: 213–232. https://doi.org/10.1007/978-1-4939-7649-2_14.

Muppirala, A. N., L. E. Limbach, E. F. Bradford, and S. C. Petersen. 2021. "Schwann Cell Development: From Neural Crest to Myelin Sheath." *Wiley Interdiscip Rev Dev Biol* 10, no. 5: e398. https://doi.org/10.1002/wdev.398.

Namini, M. S., F. Daneshimehr, N. Beheshtizadeh, et al. 2023. "Cell-free Therapy Based on Extracellular Vesicles: A Promising Therapeutic Strategy for Peripheral Nerve Injury." *Stem Cell Res Ther* 14, no. 1: 254. https://doi.org/10.1186/s13287-023-03467-5.

Niharika, L., A. Ureka, and S. K. Patra. 2024. "Dissecting SOX2 Expression and Function Reveals an Association With Multiple Signaling Pathways During Embryonic Development and in Cancer Progression." *Biochim Biophys Acta Rev Cancer* 1879, no. 5: 189136. https://doi.org/10.1016/j.bbcan.2024.189136.

Nocera, G., and C. Jacob. 2020. "Mechanisms of Schwann Cell Plasticity Involved in Peripheral Nerve Repair After Injury." *Cellular and Molecular Life Sciences* 77, no. 20: 3977–3989. https://doi.org/10.1007/s00018-020-03516-9.

O'Brien, K., K. Breyne, S. Ughetto, L. C. Laurent, and X. O. Breakefield. 2020. "RNA Delivery by Extracellular Vesicles in Mammalian Cells and Its Applications." *Nature Reviews Molecular Cell Biology* 21, no. 10: 585–606. https://doi.org/10.1038/s41580-020-0251-y.

Okonechnikov, K., A. Conesa, and F. García-Alcalde. 2016. "Qualimap 2: Advanced Multi-sample Quality Control for High-throughput Sequencing Data." *Bioinformatics* 32, no. 2: 292–294. https://doi.org/10.1093/bioinformatics/btv566.

Oliveira, J. T., C. Yanick, N. Wein, and C. E. Gomez Limia. 2023. "Neuron-Schwann Cell Interactions in Peripheral Nervous System Homeostasis, Disease, and Preclinical Treatment." *Front Cell Neurosci* 17: 1248922. https://doi.org/10.3389/fncel.2023.1248922.

Orkwis, J. A., A. K. Wolf, Z. J. Mularczyk, et al. 2022. "Mechanical Stimulation of a Bioactive, Functionalized PVDF-TrFE Scaffold Provides Electrical Signaling for Nerve Repair Applications." *Biomater Adv* 140: 213081. https://doi.org/10.1016/j.bioadv.2022.213081.

Orkwis, J. A., A. K. Wolf, S. M. Shahid, C. Smith, L. Esfandiari, and G. M. Harris. 2020. "Development of a Piezoelectric PVDF-TrFE Fibrous Scaffold to Guide Cell Adhesion, Proliferation, and Alignment." *Macromolecular Bioscience* 20, no. 9: 2000197. https://doi.org/10.1002/mabi.202000197.

Pandey, S., and J. Mudgal. 2022. "A Review on the Role of Endogenous Neurotrophins and Schwann Cells in Axonal Regeneration." *J Neuroimmune Pharmacol* 17, no. 3-4: 398–408. https://doi.org/10.1007/s11481-021-10034-3.

Parkinson, D. B., A. Bhaskaran, A. Droggiti, et al. 2004. "Krox-20 Inhibits Jun-NH2-terminal Kinase/c-Jun to Control Schwann Cell Proliferation and Death." *Journal of Cell Biology* 164, no. 3: 385–394. https://doi.org/10.1083/jcb.200307132.

Parrinello, S., I. Napoli, S. Ribeiro, et al. 2010. "EphB Signaling Directs Peripheral Nerve Regeneration Through Sox2-dependent Schwann Cell Sorting." *Cell* 143, no. 1: 145–155. https://doi.org/10.1016/j.cell.2010.08.039.

Patro, R., G. Duggal, M. I. Love, R. A. Irizarry, and C. Kingsford. 2017. "Salmon Provides Fast and Bias-aware Quantification of Transcript Expression." *Nature Methods* 14, no. 4: 417–419. https://doi.org/10.1038/nmeth.4197.

Pertea, M., G. M. Pertea, C. M. Antonescu, T. C. Chang, J. T. Mendell, and S. L. Salzberg. 2015. "StringTie Enables Improved Reconstruction of a Transcriptome From RNA-seq Reads." *Nature Biotechnology* 33, no. 3: 290–295. https://doi.org/10.1038/nbt.3122.

Poling, H. M., A. Singh, S. Kongsomros, et al. 2026. "Promoting Human Intestinal Organoid Formation and Stimulation Using Piezoelectric Nanofiber Matrices." *Tissue Engineering Part A* ahead of print, November 18. 00. https://doi.org/10.1177/19373341251396119.

Qiu, K., W. Zou, Z. Fang, et al. 2023. "2D MoS(2) and BN Nanosheets Damage Mitochondria Through Membrane Penetration." *ACS Nano* 17, no. 5: 4716–4728. https://doi.org/10.1021/acsnano.2c11003.

Quinlan, A. R., and I. M. Hall. 2010. "BEDTools: a Flexible Suite of Utilities for Comparing Genomic Features." *Bioinformatics* 26, no. 6: 841–842. https://doi.org/10.1093/bioinformatics/btq033.

Quintes, S., and B. G. Brinkmann. 2017. "Transcriptional Inhibition in Schwann Cell Development and Nerve Regeneration." *Neural Regen Res* 12, no. 8: 1241–1246. https://doi.org/10.4103/1673-5374.213537.

Rasband, M. N., and E. Peles. 2021. "Mechanisms of Node of Ranvier Assembly." *Nature Reviews Neuroscience* 22, no. 1: 7–20. https://doi.org/10.1038/s41583-020-00406-8.

Reigle, J., D. Secic, J. Biesiada, et al. 2021. "Tobacco Smoking Induces Metabolic Reprogramming of Renal Cell Carcinoma." *Journal of Clinical Investigation* 131, no. 1: e140522. https://doi.org/10.1172/jci140522.

Rigoni, M., and S. Negro. 2020. "Signals Orchestrating Peripheral Nerve Repair." *Cells* 9, no. 8: 1768. https://doi.org/10.3390/cells9081768.

Sayols, S., D. Scherzinger, and H. Klein. 2016. "dupRadar: a Bioconductor Package for the Assessment of PCR Artifacts in RNA-Seq Data." *BMC Bioinformatics [Electronic Resource]* 17, no. 1: 428. https://doi.org/10.1186/s12859-016-1276-2.

Sharma, M., M. Sheth, H. M. Poling, D. Kuhnell, S. M. Langevin, and L. Esfandiari. 2023. "Rapid Purification and Multiparametric Characterization of Circulating Small Extracellular Vesicles Utilizing a Label-free Lab-on-a-chip Device." *Scientific Reports* 13, no. 1: 18293. https://doi.org/10.1038/s41598-023-45409-4.

Sherman, B. T., M. Hao, J. Qiu, et al. 2022. "DAVID: a Web Server for Functional Enrichment Analysis and Functional Annotation of Gene Lists (2021 update)." *Nucleic Acids Research* 50, no. W1: W216–w221. https://doi.org/10.1093/nar/gkac194.

Sheth, M., M. Sharma, S. Kongsomros, et al. 2025. "Matrix Stiffness Modulated Release of Spheroid-derived Extracellular Vesicles and Discovery of Piezo1 Cargo." *BioRxiv* Preprint, posted January 17, 2025.

Shi, L., and L. Esfandiari. 2022. "A Label-free and Low-power Microelectronic Impedance Spectroscopy for Characterization of Exosomes." *PLoS ONE* 17, no. 7: e0270844. https://doi.org/10.1371/journal.pone.0270844.

Shi, L., D. Kuhnell, V. J. Borra, S. M. Langevin, T. Nakamura, and L. Esfandiari. 2019. "Rapid and Label-free Isolation of Small Extracellular Vesicles From Biofluids Utilizing a Novel Insulator Based Dielectrophoretic Device." *Lab on A Chip* 19, no. 21: 3726–3734. https://doi.org/10.1039/c9lc00902g.

Shi, L., A. Rana, and L. Esfandiari. 2018. "A Low Voltage Nanopipette Dielectrophoretic Device for Rapid Entrapment of Nanoparticles and Exosomes Extracted From Plasma of Healthy Donors." *Scientific Reports* 8, no. 1: 6751. https://doi.org/10.1038/s41598-018-25026-2.

Song, C., S. Li, Y. Mai, et al. 2024. "Dysregulated Expression of miR-140 and miR-122 Compromised Microglial Chemotaxis and Led to Reduced

Restriction of AD Pathology." *J Neuroinflammation* 21, no. 1: 167. https://doi.org/10.1186/s12974-024-03162-z.

Sticht, C., C. De La Torre, A. Parveen, and N. Gretz. 2018. "miRWalk: An Online Resource for Prediction of microRNA Binding Sites." *PLoS ONE* 13, no. 10: e0206239.

Suarez-Arnedo, A., F. Torres Figueroa, C. Clavijo, P. Arbeláez, J. C. Cruz, and C. Muñoz-Camargo. 2020. "An Image J Plugin for the High Throughput Image Analysis of in Vitro Scratch Wound Healing Assays." *PLoS ONE* 15, no. 7: e0232565. https://doi.org/10.1371/journal.pone.0232565.

Subramanian, A., P. Tamayo, V. K. Mootha, et al. 2005. "Gene Set Enrichment Analysis: A Knowledge-based Approach for Interpreting Genome-wide Expression Profiles." *PNAS* 102, no. 43: 15545–15550. https://doi.org/10.1073/pnas.0506580102.

Tang, D., M. Chen, X. Huang, et al. 2023. "SRplot: A Free Online Platform for Data Visualization and Graphing." *PLoS ONE* 18, no. 11: e0294236.

Wang, L., S. Wang, and W. Li. 2012. "RSeQC: Quality Control of RNA-seq Experiments." *Bioinformatics* 28, no. 16: 2184–2185.

Wei, Q., Y. Tu, L. Zuo, et al. 2020. "MiR-345-3p Attenuates Apoptosis and Inflammation Caused by Oxidized Low-density Lipoprotein by Targeting TRAF6 via TAK1/p38/NF-kB Signaling in Endothelial Cells." *Life Sciences* 241: 117142. https://doi.org/10.1016/j.lfs.2019.117142.

Welsh, J. A., D. C. I. Goberdhan, L. O'Driscoll, et al. 2024. "Minimal Information for Studies of Extracellular Vesicles (MISEV2023): From Basic to Advanced Approaches." *Journal of Extracellular Vesicles* 13, no. 2: e12404. https://doi.org/10.1002/jev2.12404.

Wiklander, O. P., D. R. Mamand, D. K. Mohammad, et al. 2024. "Antibody-displaying Extracellular Vesicles for Targeted Cancer Therapy." *Nature biomedical engineering* 8: 1–16.

Wong, F. C., L. Ye, I. E. Demir, and C. Kahlert. 2022. "Schwann Cell-derived Exosomes: Janus-faced Mediators of Regeneration and Disease." *Glia* 70, no. 1: 20–34. https://doi.org/10.1002/glia.24087.

Wu, X., L. Wang, M. Cong, et al. 2020. "Extracellular Vesicles From Skin Precursor-derived Schwann Cells Promote Axonal Outgrowth and Regeneration of Motoneurons via Akt/mTOR/p70S6K Pathway." *Annals of translational medicine* 8, no. 24: 1640. https://doi.org/10.21037/atm-20-5965.

Xia, B., J. Gao, S. Li, et al. 2019. "Extracellular Vesicles Derived From Olfactory Ensheathing Cells Promote Peripheral Nerve Regeneration in Rats." *Front Cell Neurosci* 13: 548. https://doi.org/10.3389/fncel.2019.00548.

Xia, B., J. Gao, S. Li, et al. 2020. "Mechanical Stimulation of Schwann Cells Promote Peripheral Nerve Regeneration via Extracellular Vesicle-mediated Transfer of microRNA 23b-3p." *Theranostics* 10, no. 20: 8974–8995. https://doi.org/10.7150/thno.44912.

Yang, E., R. Xu, L. Tu, et al. 2025. "Single Cell Deciphering of Pruritic Keloids: the Interaction Between Fibroblasts and Schwann Cells Through the Midkine Signaling." *Burns Trauma* 13: tkaf057. https://doi.org/10.1093/burnst/tkaf057.

Yao, Y., and C. Wang. 2020. "Dedifferentiation: Inspiration for Devising Engineering Strategies for Regenerative Medicine." *NPJ Regen Med* 5: 14. https://doi.org/10.1038/s41536-020-00099-8.

Yuan, M., A. Da Silva, A. Arnold, et al. 2018. "MicroRNA (miR) 125b Regulates Cell Growth and Invasion in Pediatric Low Grade Glioma." *Scientific Reports* 8, no. 1: 12506. https://doi.org/10.1038/s41598-018-30942-4.

Zhang, S., X. Xiong, and Y. Sun. 2020. "Functional Characterization of SOX2 as an Anticancer Target." *Signal Transduct Target Ther* 5, no. 1: 135. https://doi.org/10.1038/s41392-020-00242-3.

Zhao, Z., H. Wijerathne, A. K. Godwin, and S. A. Soper. 2021. "Isolation and Analysis Methods of Extracellular Vesicles (EVs)." *Extracell Vesicles Circ Nucl Acids* 2, no. 1: 80–103. https://doi.org/10.20517/evcna.2021.07.

Zhou, S., D. Shen, Y. Wang, et al. 2012. "microRNA-222 Targeting PTEN Promotes Neurite Outgrowth From Adult Dorsal Root Ganglion Neurons Following Sciatic Nerve Transection." *PLoS ONE* 7, no. 9: e44768. https://doi.org/10.1371/journal.pone.0044768.

Zhu, S., L. Chen, M. Wang, et al. 2023. "Schwann Cell–derived Extracellular Vesicles as a Potential Therapy for Retinal Ganglion Cell Degeneration." *Journal of Controlled Release* 363: 641–656.

Zhuang, W., H. Liu, Z. He, et al. 2022. "miR-92a-2-5p Regulates the Proliferation and Differentiation of ASD-Derived Neural Progenitor Cells." *Current Issues in Molecular Biology* 44, no. 6: 2431–2442. https://doi.org/10.3390/cimb44060166.

Zou, W., M. Lai, Y. Jiang, et al. 2023. "Exosome Release Delays Senescence by Disposing of Obsolete Biomolecules." *Adv Sci (Weinh)* 10, no. 8: e2204826. https://doi.org/10.1002/advs.202204826.

Zou, Y. 2023. "Establishment of an in Vitro Differentiation and Dedifferentiation System of Rat Schwann Cells." *Bio Protoc* 13, no. 5: e4631. https://doi.org/10.21769/BioProtoc.4631.

Zou, Y., S. Wu, F. Wen, Y. Ge, and S. Luo. 2023. "PGC-1α Inhibits Schwann Cell Dedifferentiation and Delays Peripheral Nerve Degeneration by Targeting PON1." *Cellular and Molecular Neurobiology* 43, no. 7: 3767–3781. https://doi.org/10.1007/s10571-023-01395-9.

Supporting Information

Additional supporting information can be found online in the Supporting Information section.

Supporting Information: jex270157-sup-0001-TableS1-S11.xlsx **Supporting Information**: jex270157-sup-0002-FigureS1-S11.docx